https://doi.org/10.5194/acp-2019-773
Preprint. Discussion started: 20 September 2019

Atmospheric Chemistry and Physics Discussions

Characterization of Organic Aerosol across the Global Remote Troposphere: A comparison of ATom measurements and global chemistry models

Alma Hodzic[1], Pedro Campuzano-Jost[2,3], Huisheng Bian[4], Mian Chin[4], Peter R. Colarco[4], Douglas A. Day[2,3], Karl D. Froyd[2,8], Bernd Heinold[6], Duseong S. Jo[2,3], Joseph M. Katich[2,8], Jack K. Kodros[5], Benjamin A. Nault[2,3], Jeffrey R. Pierce[5], Eric Ray[2,8], Jacob Schacht[6], Gregory P. Schill[2,8], Jason C. Schroder[2,3], Joshua P. Schwarz[2,8], Dianna T. Sueper[2,3], Ina Tegen[6], Simone Tilmes[1], Kostas Tsigaridis[7,8], Pengfei Yu[9,10], Jose L. Jimenez[2,3]

[1]National Center for Atmospheric Research, Boulder, CO, USA

[2]Cooperative Institute for Research in Environmental Sciences (CIRES), University of Colorado, Boulder, CO, USA

[3]Department of Chemistry, University of Colorado, Boulder, CO, USA

[4]NASA Goddard Space Flight Center, Greenbelt, MD, USA

[5]Department of Atmospheric Science, Colorado State University, Fort Collins, CO, USA

[6]Leibniz Institute for Tropospheric Research, Leipzig, Germany

[7]Center for Climate Systems Research, Columbia University, New York, NY, USA

[8]NASA Goddard Institute for Space Studies, New York, NY, USA

[9]NOAA Earth System Research Laboratory (ESRL), Chemical Sciences Division, Boulder, CO, USA

[10]Institute for Environmental and Climate Research, Jinan University, Guangzhou, Guangdong, China

Key words: organic aerosol, remote atmosphere, ATom field campaign.

https://doi.org/10.5194/acp-2019-773
Preprint. Discussion started: 20 September 2019

Atmospheric Chemistry and Physics Discussions

Abstract.

The spatial distribution and properties of submicron organic aerosols (OA) are among the key sources of uncertainty in our understanding of aerosol effects on climate. Uncertainties are particularly large over remote regions of the free troposphere and Southern Ocean, where very little data has been available, and where OA predictions from AeroCom Phase II global models span a factor of 400-1000, greatly exceeding the model spread over source regions. The (nearly) pole-to-pole vertical distribution of non-refractory aerosols was measured with an aerosol mass spectrometer onboard the NASA DC8 aircraft as part of the Atmospheric Tomography (ATom) mission during the northern hemisphere summer (August 2016) and winter (February 2017). This study presents the first extensive characterization of OA mass concentrations and their level of oxidation in the remote atmosphere. OA and sulfate are the major contributors by mass to submicron aerosols in the remote troposphere, together with sea salt in the marine boundary layer. Sulfate was dominant in the lower stratosphere. OA concentrations have a strong seasonal and zonal variability, with the highest levels measured in the summer and over the regions influenced by the biomass burning from Africa (up to 10 μg sm^{-3}). Lower concentrations (~0.1-0.3 μg sm^{-3}) are observed in the northern mid- and high- latitudes and very low concentrations (< 0.1 μg sm^{-3}) in the southern mid- and high- latitudes. The ATom dataset is used to evaluate predictions of eight current global chemistry models that implement a variety of commonly used representations of OA sources and chemistry, as well as of the AeroCom-II ensemble. The current model ensemble captures the average vertical and spatial distribution of measured OA concentrations, and the spread of the individual models remains within a factor of 5. These results are significantly improved over the AeroCom-II model ensemble, which shows large overestimations over these regions. However, some of the improved agreement with observations occurs for the wrong reasons, as models have the tendency to greatly overestimate the primary OA fraction, and underestimate the secondary fraction. Measured OA in the remote free troposphere are highly oxygenated with organic aerosol to organic carbon (OA/OC) ratios of ~ 2.2-2.8 and are 30-60% more oxygenated than in current models, which can lead to significant errors in OA concentrations. The model/measurement comparisons presented here support the concept of a more dynamic OA system as proposed by Hodzic et al. (2016), with enhanced removal of primary OA, and a stronger production of secondary OA in global models needed to provide a better agreement with observations.

https://doi.org/10.5194/acp-2019-773
Preprint. Discussion started: 20 September 2019

1 Introduction

Organic aerosols (OA) are a complex mixture of directly emitted primary OA (POA) and chemically produced secondary OA (SOA) from anthropogenic and biogenic emission sources. They are associated with adverse health effects (Mauderly and Chow, 2008, Shiraiwa et al., 2017) and a major contribution to radiative forcing in the climate system (Boucher et al., 2013). The currently limited understanding of processes involved in the formation, ageing, and removal of organic compounds results in large uncertainties in (i) the predicted global OA burden, (ii) relative contributions of emissions vs. chemistry to OA formation, (iii) spatial distribution, and (iv) impacts on radiation and clouds (Kanakidou et al., 2005, Hallquist et al., 2009, Heald et al., 2011, Spracklen et al., 2011, Tsigaridis et al., 2014, Hodzic et al., 2016, Shrivastava et al., 2017, Tsigaridis and Kanakidou, 2018). The uncertainties are particularly large in the estimated global burden of SOA that range from 12 to 450 Tg y^{-1} (see Fig. 9 of Hodzic et al., 2016), and in their direct and indirect radiative forcing that range from -0.08 to -0.33 W m^{-2}, and -0.60 to −0.77 W m^{-2}, respectively (Spracklen et al., 2011, Myhre et al., 2013, Scott et al., 2014, Hodzic et al., 2016, Tsigaridis and Kanakidou, 2018). Reducing these uncertainties is becoming more important as OA is on a path to becoming the dominant fraction of the submicron anthropogenic aerosol mass globally due to the ongoing efforts to reduce SO_2 emissions and associated sulfate aerosols.

Model performance has been especially poor in the remote regions of the atmosphere where OA measurements available for model evaluation have been sparse (especially aloft). Using data from 17 aircraft campaigns mostly located in the northern hemisphere Heald et al. (2011) showed that the skill of the global GEOS-Chem model in predicting the vertical distribution of OA was significantly decreased in remote regions compared to polluted near-source regions. The study pointed out the limitations of commonly used SOA formation mechanisms that are based on chamber data; these have the tendency to underpredict OA in source regions and overpredict OA in the remote troposphere. For the same field campaigns, Hodzic et al. (2016) showed that OA is likely a more dynamic system than represented in chemistry-climate models, with both stronger production and stronger removals. These authors suggested that additional removal mechanisms via e.g. photolytic or heterogeneous reactions of OA particles are needed to explain low OA concentrations observed in the upper troposphere where direct cloud scavenging is less efficient. The recent global multi-model comparison study (Tsigaridis et al., 2014) within

https://doi.org/10.5194/acp-2019-773
Preprint. Discussion started: 20 September 2019

the AeroCom Phase II project illustrates well the amplitude of model uncertainties simulating OA mass concentrations and the contrast in model performance between near-source and remote regions. The results indicate that model dispersion (the spread between the models with the lowest and highest predicted OA concentrations) increases with altitude from roughly 1 order of magnitude near the surface to 2-3 orders of magnitude in the upper troposphere. Our own analyses of the AeroCom-II results shown in Figure 1a indicate that model dispersion increases not only with altitude but also with distance from the northern mid-latitude source (and data-rich) regions. The model spread is a factor of 10-20 in the free troposphere between the equator and northern mid-latitudes, and increases to a factor of 200-800 over the Southern Ocean and near the tropopause. It is not surprising that model spread is lower closer to source regions where it is mostly driven by uncertainties in emissions and SOA production yields. Spread is expected to be larger in remote regions where models are also impacted by uncertainties in transport, chemical ageing and removal. The lowest model dispersion also coincides with the regions of the northern hemisphere (NH) or the African biomass burning outflow where models have been evaluated the most (Figure 1b), emphasizing the need for further model/observation comparison studies in remote regions (of the southern hemisphere (SH) in particular).

Here, we present a unique data set of airborne aerosol mass spectrometer measurements of OA mass concentrations collected onboard the NASA DC-8 as part of the Atmospheric Tomography (ATom) mission. The aircraft sampled the vertical structure of the atmosphere from near-surface (0.2 km) to the lower-stratosphere (LS) regions (12 km altitude) over both the Pacific and Atlantic basins (to limit the influence of source regions) with a quasi-global spatial coverage from 82°N to 67°S. This dataset is used to perform the first systematic global-scale multi-model evaluation of the chemistry-climate models focusing on OA in the remote troposphere over the remote oceans. We focus on the NH summer (August 2016, ATom-1) and NH winter (February 2017, ATom-2) deployments. Overall these ATom missions sampled the marine boundary layer (MBL) for 10% of the flight tracks, 12% of the time the remote lower stratosphere, and the rest the free troposphere. The model-observation comparisons are aimed at identifying discrepancies in terms of OA mass concentrations and vertical distribution, their fractional contribution to submicron aerosols, and their oxidation level in global models.

The modeling framework is described in Section 2. Section 3 describes the ATom dataset and the spatial and vertical distributions of OA over the Atlantic and Pacific regions.

https://doi.org/10.5194/acp-2019-773
Preprint. Discussion started: 20 September 2019

Section 4 presents the comparisons of ATom-1 and -2 data to multi-model predictions from both the AeroCom-II models, and the ensemble of eight current model simulations of the ATom campaign. Section 5 presents the conclusions of the study and discusses its implications.

2 Modeling framework

2.1 ATom models

ATom measurements were compared with results of eight global models that simulated the time period of the ATom-1 and 2 campaigns (August 2016 and February 2017), using reanalysis meteorology (and a spin-up time of at least six to twelve months). These are referred hereafter as ATom models and include the NASA global Earth system model GEOS5-GOCART, the aerosol-climate model ECHAM-HAM, three versions of the NCAR Community Earth System Model (CESM), and three versions of the global chemistry GEOS-Chem model. Simulations were performed at various horizontal resolutions ranging from relatively high ~50km (GEOS5-GOCART) and ~100km (CESM2 models) resolutions to somewhat coarser grids of ~200km (CESM1-CARMA, GEOS-Chem) and ~400km for GC10-TOMAS. The advantage of using the same host model (in the cases of variants of CESM2 and GEOS-Chem) is that the dynamics and emissions remain comparable. Models differ greatly in their treatment of emissions, gas-phase chemistry, aerosol chemistry and physical processes, and aerosol coupling with radiation and clouds, among others. Table 1 describes the configuration of various models (e.g. meteorology, emissions), and their treatment of OA. In this section we only summarize the main features and parameters directly impacting the OA simulations. Some models do not include SOA chemistry and instead assume that SOA is directly emitted proportional to the emissions of its precursors (ECHAM6-HAM, CESM2-SMP, GEOS5-GOCART, GC10-TOMAS), while others have more complex treatments of organic compounds, their chemistry, and partitioning into particles (GC12-REF, GC12-DYN, GC10-TOMAS, CESM1-CARMA, CESM2-DYN). It should be noted that models that directly emit SOA assume that SOA is a non-volatile species that remains irreversibly in the particle phase. There are some commonalities between simulations for the treatment of biogenic emissions, which are based in all models on the Model of Emissions of Gases and Aerosols from Nature (MEGAN, Guenther et al., 2012) to generate meteorology-dependent emissions of volatile organic compounds. None of the models includes the marine production of OA which is estimated to be ~3 orders of magnitude smaller than the continental production of OA from

https://doi.org/10.5194/acp-2019-773
Preprint. Discussion started: 20 September 2019

both isoprene and monoterpene precursors (Kim et al., 2017). This contribution could however be larger for sea-spray biological material from phytoplankton with predicted contributions of 0.01 to 0.1 μg m^{-3} to surface submicron aerosol over remote oceanic regions (Vergara-Temprado et al., 2017, Middlebrook et al., 1998). Below we only provide a brief description of most important processes that influence OA for each model.

GEOS5-GOCART was run in a configuration similar to Bian et al. (2019) using the anthropogenic emissions from HTAP v2 (Janssens-Maenhout et al., 2015) and biomass burning emissions from the Quick Fire Emission Dataset (QFED v2.54). Aerosols are simulated within the GOCART bulk aerosol module and include externally mixed particles of black carbon (BC), organic carbon (OC), sulfate, ammonium, nitrate, dust and sea salt (Colarco et al., 2010, Bian et al., 2017). The formation of SOA is based on a prescribed 10% formation yield from the monoterpene emissions. The primary emitted OC and SOA are separated into hydrophobic (50%) and hydrophilic (50%) species, with a 2.5 days e-folding time conversion from hydrophobic to hydrophilic organic particles. Both types of organic particles are dry deposited, while the hydrophilic organic fraction undergoes rain scavenging in convective updrafts, and in large-scale precipitation.

The ECHAM-HAM version ECHAM6.3-HAM2.3 (Tegen et al., 2019) was run using updated anthropogenic emissions (Schacht et al, 2019) combining the ECLIPSE (Klimont et al., 2017) emissions, with the Russian anthropogenic BC emissions from Huang et al. (2015). For biomass burning the Global Fire Assimilation System (GFAS, Kaiser et al., 2012) biomass burning emissions are used, however, without the scaling factor of 3.4 suggested by Kaiser et al. (2012). Aerosol composition and processes are simulated using the Hamburg Aerosol Model (HAM2, Zhang et al., 2012), that considers an aerosol internal mixture of sulfate, BC, OC, sea salt, and mineral dust. The aerosol population and their microphysical interactions are simulated using seven log-normal modes, including the nucleation mode, soluble and insoluble Aitken, accumulation and coarse modes. In the model configuration used in this publication the formation of SOA is based on a prescribed 15% mass yield from monoterpene emissions only (Dentener et al., 2006).

The two simulations with the GEOS-Chem 12.0.1 global chemistry model (Bey et al., 2001) use emissions based on CMIP6 global inventory with regional improvements for anthropogenic sources, and on GFED v.4 for biomass burning emissions (Giglio et al., 2013). Both simulations use the bulk aerosol representation and differ only in the treatment of SOA formation and removal. The first configuration (called hereafter GC12-REF)

https://doi.org/10.5194/acp-2019-773
Preprint. Discussion started: 20 September 2019

includes the default (http://wiki.seas.harvard.edu/geos-chem/index.php) representation of SOA formation based on the volatility basis set (VBS) of Pye et al. (2010), and the isoprene SOA formation based on Marais et al. (2016). The second configuration (referred to as GC12-DYN) includes a more dynamic representation of the SOA lifecycle based on Hodzic et al. (2016), with the exception of the treatment of isoprene SOA that is formed in the aqueous aerosols as in Marais et al. (2016). As in Hodzic et al. (2016) the GC12-DYN model version includes updated VBS SOA parameterization, updated dry and wet removal of organic vapors, and photolytic removal of SOA. SOA formation is based on wall-corrected chamber yields (Zhang et al., 2014) for the traditional precursors (isoprene, monoterpenes, sesquiterpenes, benzene, toluene, xylene) and on yields derived from an explicit chemical mechanism for higher molecular weight n-alkanes and n-alkenes species (Hodzic et al., 2016). The removal of gas-phase oxidized volatile organics uses updated Henry's law solubility coefficients from Hodzic et al. (2014), and photolytic removal of SOA (Hodzic et al., 2015). In addition to OA, the model includes BC and dust, and simulates the chemistry and gas-particle partitioning of inorganic compounds such as sulfate, ammonium, nitrate and sea salt using the ISORROPIA II thermodynamic model (Fountoukis and Nenes, 2007). In both GEOS-Chem configurations, BC and primary OC are simulated with a hydrophobic and hydrophilic fraction for each. At the time of emission, 80% of BC and 50% of primary OC are considered as hydrophobic. Hydrophobic aerosols are converted to hydrophilic aerosols with an e-folding lifetime of 1.15 days. An OA/OC ratio of 2.1 is assumed to convert POC to POA, and SOA is simulated as OA mass (i.e. no OA/OC ratio assumption is needed for SOA, except for comparison with OC measurements). Soluble gases and aerosols are removed by both dry and wet deposition. Wet deposition includes scavenging in convective updrafts, and in-cloud and below-cloud scavenging from large-scale precipitation (Liu et al., 2001). Hydrophobic aerosols (BC and POA) are scavenged in convective updrafts following Wang et al. (2014).

GC10-TOMAS is based on the GEOS-Chem version 10.01 coupled with TwO Moment Aerosol Sectional microphysics scheme (TOMAS) and ran in a similar configuration to that described in Kodros et al. (2016). The model computes the evolution of sulfate, sea salt, primary and secondary OA, BC, and dust aerosols described by 15 internally mixed size bins (of which six were analyzed for these comparisons, cf. Table 1). Anthropogenic emissions are based on the EDGAR v4 global inventory with regional improvements, while the biomass burning emissions are from GFED v3. SOA are irreversibly made from the

https://doi.org/10.5194/acp-2019-773
Preprint. Discussion started: 20 September 2019

emitted parent precursor, considering a 10% mass yield from monoterpene emissions, and an emission flux of 0.2 Tg of SOA per Tg of CO for the anthropogenic CO emissions.

Simulations based on the CESM2.0 Earth system model use the Whole Atmosphere Community Climate Model (WACCM6, Gettelman et al., 2019, Emmons et al., 2019). Details on the specific of the model configurations are described in detail in Tilmes et al. (2019) i.e. CESM2-SMP and CESM2-DYN correspond to the specified dynamics WACCM6-SOAG and WACCM6-VBSext simulations described in that work, respectively. Emissions are based on the CMIP6 global inventory for the year 2014 for anthropogenic sources, and on the QFED version 2.4 for the wildfires inventory. Aerosols are represented with the modal aerosol scheme (MAM4, Liu et al., 2012) that includes BC, primary and secondary OA, sulfate, dust and sea salt. Four modes are considered including Aitken, accumulation and coarse size modes, and an additional primary carbon mode. Only the accumulation mode was used in this work. The CESM2-SMP and CESM2-DYN simulations differ in their treatment of OA. CESM2-SMP forms OA directly using fixed mass yields from primary emitted precursors (isoprene, monoterpenes, aromatics) without explicitly simulating their oxidation and partitioning. These mass yields are increased by a factor of 1.5 to match the anthropogenic aerosol indirect forcing (Liu et al., 2012). The second configuration (referred to as CESM2-DYN) includes the formation and removal parameterizations of organics of Hodzic et al. (2016), as implemented into CESM2 by Tilmes et al. (2019) for all species based on low-NOx VBS yields only. This is a similar SOA scheme as used in GC12-DYN (with the exception of the detailed isoprene-SOA scheme that is included in GC12-DYN). Organic gases and aerosols undergo dry and wet deposition as described in Liu et al. (2012). It should be noted that CESM2-SMP does not include deposition of intermediate organic vapors. Aerosol wet scavenging considers in-cloud scavenging (the removal of cloud-borne particles that were activated at the cloud base) and below-cloud scavenging for both convective and grid-scale clouds.

CESM1-CARMA simulations use the configuration described in Yu et al. (2019) which is based on CESM1 and the sectional Community Aerosol and Radiation Model for Atmospheres (CARMA v3.0). Anthropogenic emissions are those from the Greenhouse gas-Air pollution Interactions and Synergies (GAINS) model, and biomass burning emissions are from the Global Fire Emission Database (GFED v3, van der Werf et al., 2010). In CARMA, 20 size bins are used for both pure sulfate particles (bins from 0.2 nm to 1.3 μm in radius, only used up to 500 nm) and mixed aerosols composed of BC, primary

https://doi.org/10.5194/acp-2019-773
Preprint. Discussion started: 20 September 2019

and secondary OC, dust, sea salt, and sea-spray sulfate (bins from 0.05–8.7 μm in radius, again, only analyzed up to 500 nm). SOA formation is based on the VBS approach from Pye et al. (2010). The removal of OA occurs only by dry and wet deposition. Compared to the CESM2-SMP and CESM2-DYN simulations, the convective removal of aerosols uses the modified scheme described in Yu et al. (2019) which accounts for aerosol secondary activation from the entrained air above the cloud base, and the scavenging of activated aerosols in convective updrafts. The default CESM can transport aerosols from the cloud base to the top of the cloud in strong convective updrafts in one time step without scavenging them, while the new scheme allows for a more efficient removal off all aerosols inside convective clouds. A sensitivity simulation is performed for ATom-1 to quantify the effect of this improved removal on OA concentrations (Section 4.5).

2.2 AeroCom-II models

The ATom measurements are also compared in a climatological way to the global model OA predictions generated within the Phase II Aerosol Comparisons between Observations and Models (AeroCom-II) project (Schulz et al., 2009). We consider the results of 28 global models, which is a subset of those presented in Tsigaridis et al. (2014), based on the availability of model results. It should be noted that the meteorological forcing used in these models is mostly based on the year 2006, while the anthropogenic and biomass burning emissions are mostly representative of the year 2000. For comparison purposes, the monthly mean model outputs for the months of August (ATom-1) and February (ATom-2) are interpolated along the flight path (latitude, longitude, and altitude), and averaged the same way as the measurements (see section 3.2).

3 Description of ATom measurements

3.1 Submicron aerosol data

The measurements of non-refractory submicron aerosols were performed onboard the NASA DC8 aircraft as part of the ATom field study (Wofsy et al., 2018) using the University of Colorado Aerodyne High-Resolution Time-of-Flight Aerosol Mass Spectrometer (AMS in the following, Canagaratna et al., 2007, DeCarlo et al., 2006).

We use measurements from both the NH summer (August 2016, ATom-1) and winter (February 2017, ATom-2) deployments. Figure 2a shows the flight path and the vertical extent of the ATom-1 dataset colored by OA mass concentrations (see Figure S1 for ATom-2). The aircraft performed systematic vertical sampling with ~140 vertical profiles

https://doi.org/10.5194/acp-2019-773
Preprint. Discussion started: 20 September 2019

per campaign throughout the troposphere from the near surface ~0.2 km to the upper troposphere/lower stratosphere region at ~13 km altitude. Details on the operation of the CU AMS on board the DC-8 are reported in Schroder et al. (2018), Nault et al. (2018), and Guo et al. (2019). For ATom, the AMS reported the standard non-refractory aerosol species OA, sulfate, nitrate, ammonium, and chloride, with the response for all the nominally inorganic species characterized by in-field calibrations. In addition, it also reported methanesulfonic acid (MSA, Hodshire et al., 2019a describes the AMS MSA methods and calibrations for ATom) and sea salt for for D_{geo}<450 nm (based on the method of Ovadnevaite et al., 2012). Both of these species were important to achieve closure with the volume calculated from the on-board sizing instruments in the marine boundary layer (Guo et al., 2019). Another important refractory submicron species not captured by the AMS measurements is BC. This was measured on ATom with the NOAA SP2 instrument (Katich et al., 2018). It should be noted that aircraft measurements of aerosol mass concentrations are given in $\mu g\ sm^{-3}$ (i.e., under standard conditions of 1 atm and 273.15 K).

For ATom the AMS measured particles with geometric diameters (based on the campaign-wide average density of 1640 kg m^{-3}, Guo et al., 2019) of between D_{geo}~60 and 295 nm with ~100% efficiency (and between 35 and 460 nm with 50% efficiency). Here we denote the AMS aerosol data as “submicron” mass (based on the more usual definition using aerodynamic diameter, which is larger than the geometric diameter; DeCarlo et al., 2004), with the assumption that non-refractory aerosol are small contributors to mass above the AMS size range. As shown in Brock et al., 2019 and Guo et al., 2019, the accumulation mode for the ATom sampling environment only extended up to 500 nm, and hence, as expected for a background tropospheric environment, this approximation is appropriate. Very good agreement was observed with the integrated volume calculated from the number size distributions for ATom (Brock et al., 2019). A low bias compared to a typical submicron definition can occur in thick biomass burning plumes and in the lower stratosphere at times (Guo et al., 2019). As detailed in Table 1, the accumulation mode for the bulk models discussed in this study overlaps with the size range of the AMS, and for the sectional models (CESM1-CARMA, GEOS-Chem-TOMAS, ECHAM6-HAM) only the bins that match the AMS size range were used. As expected based on the previous discussion, however, a comparison of the total OA calculated by these sectional models with the modeled OA inside the AMS size-range showed small differences (Slopes for

https://doi.org/10.5194/acp-2019-773
Preprint. Discussion started: 20 September 2019

ATom-1 linear regressions: CARMA:0.91, TOMAS: 0.94, ECHAM6-HAM 1.00) mostly influenced by the high points in the biomass plumes off Africa).

Refractory and non-refractory aerosol composition was also measured using the NOAA Particle Analysis by Laser Mass Spectrometry (PALMS) instrument. PALMS classifies individual aerosol particles into compositional classes including biomass burning (Hudson et al., 2004), sea salt (Murphy et al., 2019), mineral dust (Froyd et al., 2019), and others. Mass concentrations for these particles types are derived by combining PALMS composition data with aerosol size distribution measurements (Froyd et al., 2019). Good agreement overall was found for OA, sulfate and seasalt between the two particle mass spectrometers during ATom once the AMS and PALMS instrument transmissions were accounted for (Guo et al., 2019). For all PALMS data used in this work (biomass burning fraction and dust) the AMS transmission function was applied.

For a particular airmass, the mass fraction of biomass burning (BB) aerosol reported by the PALMS instrument $f(BB)_{PALMS}$ (Thompson and Murphy, 2000; Froyd et al., 2019) was then used to evaluate the degree of BB influence. This parameter correlates quite well with other gas-phase BB tracers, and is more useful as a particle tracer. Importantly, it is not impacted by the long lifetimes of the gas-phase tracers (e.g. 9 months for CH_3CN) and has hence a much higher contrast ratio in the ATom dataset. An airmass was classified as non-BB influenced when $f(BB)_{PALMS}$ was lower than 0.30 (Hudson et al, 2004) as shown in Figure 2b. It was also used to assess the impact of POA on the total OA burden (next section). For ATom-1 (ATom-2), 76% (97%) of measurements were classified as not influenced by biomass burning.

3.2 Estimation of the POA fraction for the ATom dataset

For model evaluation purposes, it is important to know whether the source of OA is primary or secondary. For ground studies close to sources (e.g. Jimenez et al., 2009) Positive Matrix Factorization of AMS mass spectra (PMF, Ulbrich et al., 2009) can be used to estimate the contribution of primary sources (mostly from transportation, heating, cooking, and biomass burning) to total OA. This approach is not suitable for ATom, since the aerosol is too aged to be effectively classified into POA and SOA by PMF. However, PMF analyses can still be useful for other purposes, such as identifying MSA, as previously observed in remote environments (Hodshire et al., 2019a).

https://doi.org/10.5194/acp-2019-773
Preprint. Discussion started: 20 September 2019

Instead, in this work we have estimated POA based on the fact that it is co-emitted with BC as part of the combustion processes releasing both species in source regions, and that BC is not impacted by chemical aging processes over the lifetime of the airmass. We assume non-differential removal (and transport) of the BC fraction relative to the rest of the POA (the two are generally internally mixed, Lee et al., 2015). Table S1 summarizes recent POA/BC and POC/EC emission ratio determinations for urban background sites, which best represent real mixes of pollution sources, and for individual sources of POA (from mobile sources – commonly referred as HOA – and cooking aerosol – COA). Based on Table S1 data, we assume POA to be co-emitted with BC for anthropogenic fossil fuel / urban region POA (herein called FF_{ratio} for simplicity, even though much of it is non-fossil, Zotter et al., 2014; Hayes et al., 2015) at a ratio of 1.55 (average of all studies). Mobile source measurements in general exhibit lower ratios (POA/OA ratio 0.5-1.5) while COA determination typically ranges from 2 to 3. Hence, the ratio used here is a good estimate for a diverse mix of urban sources as appropriate for ATom. For biomass burning sources, we use a value of POA/BC = 13.5 (BB_{ratio}), based on the average of the recent review by Andreae (2019), which included over 200 previous determinations for a variety of fuels and burning conditions. We note the measured total OA/BC of ~3.5 (conservatively assuming that all OA is POA) observed on both ATom missions for the large African-sourced BB plumes over the Equatorial Atlantic. We note that using the larger BB_{ratio} from Andreae (2019) leads to a POA fraction >> 100% in the ATom African plumes. We also perform sensitivity studies with values of both FF_{ratio} and BB_{ratio} within the literature range.

The PALMS determined mass fraction of biomass impacted aerosol ($f(BB)_{PALMS}$) can then be used to determine a total POA contribution from both types of sources:

$$POA = [BC]*(FF_{ratio}+(BB_{ratio}- FF_{ratio})*f(BB)_{PALMS}) \quad \text{(Eq. 1)}$$

Further detail is provided in Table S2, which summarizes the POA/BC ratios used in the emission inventories implemented in current models. Overall, there is reasonable agreement with the measurements in Table S1, with FF_{ratio} ranging from ~0.5 for diesel fuels, to >2 for energy production and ~5 for residential emissions (which include some BB). On the other hand, for biomass burning, the emission inventories ratios range from ~5 for crop, to ~15 for forest, and up to ~50 for peatland. While generally consistent with the values discussed by Andreae (2019), they are on the lower end of the ranges discussed in that work. Overall, within the uncertainties of both the measured and model-implemented emission ratios no significant bias is apparent.

https://doi.org/10.5194/acp-2019-773
Preprint. Discussion started: 20 September 2019

PALMS detection efficiency increases with size across the accumulation mode, and therefore the f(BB) number fraction is weighted to the larger size end of the accumulation mode. In very clean regions of the upper troposphere (typically <0.15 µg sm^{-3} submicron mass) particles below the PALMS size range can contribute significantly to aerosol mass (Williamson et al., 2019; Guo et al., 2019). If BB particles are not evenly distributed across the entire accumulation mode (due to preferential removal in convective updrafts of primary aerosol, cf. Yu et al., 2019 and Section 4.5; and preferential condensation of SOA on smaller particles), then the f(BB) reported by PALMS will be an overestimation. For the final analysis these periods where left in the dataset, and therefore for the LS the reported POA is likely overestimated for these regions, although their impact on the mass-weighted campaign average is negligible.

3.3 Data processing for comparisons

For the comparisons between the measurements and the various global models, data were averaged both vertically and zonally to minimize the impact of smaller plumes or vertical gradients in aerosol concentrations that might not be captured by coarse resolution models. For the same reason, all data near airports was removed from the datasets prior to analysis (up to about 3 km on the climb in/out). In order to restrict this analysis to the remote troposphere, the last leg of the ATom-1 mission (over the continental US) was taken out of the dataset as well. Data was binned into 5 large latitude regions as shown in Figure 2a including southern polar (55-80°S, “S.Polar”), southern mid-latitudes (25-55°S, “S.Mid”), equatorial (25°S-25°N, “Equatorial”), northern mid-latitudes (25-55°N, “N.Mid”), northern polar (55-80°N, “N.Polar”) and analyzed separately for the Pacific and Atlantic basins. For data in each of these latitude regions, altitude profiles were calculated with a constant 600 m altitude resolution. According to both variability in the cleanest air and statistical analysis of the organic background subtraction (Drewnick et al. 2009), the 1σ precision at low concentrations for one-minute data ranged between 20 and 50 ng sm^{-3}, or a 3σ detection limit between 60 and 150 ng sm^{-3} for the one-minute data (confirmed by frequent filter blanks). On average, each individual point in the profiles represents the average of about 25 min of ATom flight data. At that time resolution, the OA 1σ precision was about 10 ng sm^{-3}. Hence with very few exceptions (10 points for both missions combined), the OA concentrations in the averaged profiles reported are well above the instrumental detection limit in those regions. For model-measurement comparisons along flight tracks, model outputs and measurements were considered at 1-minute time

https://doi.org/10.5194/acp-2019-773
Preprint. Discussion started: 20 September 2019

resolution, which corresponds to ~0-700 m vertical resolution and ~0.05-0.15 degrees horizontal resolution. Note that a large fraction of the 1-minute OA values in the remote free troposphere were below the local 3σ detection limit and require averaging before use. We therefore caution future data users that the reported data should be averaged as needed, as replacing below-detection limit values by other values introduces biases on averages. For fractional ratio analysis, measurements were averaged to 5-minute time resolution to reduce the noise in the ratios due to noise in the denominator. The results are not very sensitive to the 5-minute averaging (compared to 1-minute) as shown in Figure S11 for OA to sulfate ratios.

Some of the performed analysis required separating the dataset into vertical subsets. In this manuscript, we define the marine boundary layer (MBL) as the region below 1.5 times the calculated boundary layer height in the NCEP global model reanalysis. The free troposphere (FT) includes all data points between the top of MBL and the NCEP tropopause height, and the LS region includes all points above the NCEP tropopause height.

3.4 Submicron aerosol composition

Figure 2b shows that during both NH summer and winter ATom deployments, OA is one of the three dominant components of the measured submicron aerosol in the remote troposphere, together with sulfate and sea salt. During ATom-1, average submicron aerosol concentrations were close to 0.8 μg sm^{-3} in the marine boundary layer and biomass burning outflow regions, and ~2 times lower in the free troposphere and lower stratosphere regions. ATom-2 had overall lower average concentrations below 0.4 μg sm^{-3} (vs. 0.5 μg sm^{-3} for ATom-1). As expected, sulfate (sulfuric acid in the lower stratosphere) is the dominant constituent in the MBL (~50%) and LS (50-70%), while the OA contribution is generally below 10% and 40%, respectively in those regions. A large fraction of sea salt aerosol is found in the MBL especially during the NH winter deployment (~30%, see Murphy et al., 2019).

OA is found to be a major constituent (~50%) of submicron aerosol in the clean (non-BB influenced) free troposphere. The contribution of OA is 1.4 times larger than that of sulfate during the NH summer, and 1.2 times lower than that of sulfate during the NH winter, which is likely due to a large contribution of the NH sources to SOA production in the NH summer. Biomass-burning events increase the OA contribution relative to that of sulfate,

https://doi.org/10.5194/acp-2019-773
Preprint. Discussion started: 20 September 2019

and lead to a higher contribution of OA to total during the ATom-1 mission (stronger BB influence).

3.5 Spatial and vertical distribution of OA

Figure 2a (and Fig. S1) shows the spatial and vertical distribution of OA mass concentrations measured during ATom-1 (and ATom-2) campaigns. Most data were taken over remote oceanic regions (and a few remote continental regions, primarily over the Arctic). The measured OA varies between extremely clean conditions (< 0.1 μg sm^{-3}) encountered mostly in the Pacific and Southern Ocean regions and moderately polluted conditions (> 2 μg sm^{-3}) in the biomass burning outflow regions. During ATom-1 (August 2016), a strong BB influence is observed in the lower troposphere (below 6 km) over the Atlantic basin off the African coast and over California with OA concentrations exceeding 10 μg sm^{-3}. OA associated with biomass burning is also present in the upper troposphere over equatorial regions and over Alaska, associated with the deep convective transport of biomass burning aerosols. The biomass burning contribution to carbonaceous aerosols in those regions during ATom-1 was also apparent in the black carbon measurements (Katich et al., 2019). ATom-2 was generally less polluted than ATom-1 due to a more limited global influence of biomass burning emissions during that period, and also to a less active photochemistry during winter months in the NH.

The measured OA is characterized by a strong latitudinal gradient. Figure 2c shows the average vertical profiles of measured OA over the selected latitudinal bands during August 2016. The cleanest airmasses are observed over the remote oceanic regions of the Southern Hemisphere (SH, 25-80°S) with OA mass concentrations below 0.06 μg sm^{-3}. These extremely low OA concentrations can be explained by the very low influence from continental emission sources, and presumably low marine POA and SOA precursor emissions. This is consistent with low concentrations of gas-phase pollutants (e.g. CO, ethane, propane). An enhancement can be noticed above 10 km in the lower stratosphere. In some cases, this could be related to the long-range transport of biomass burning aerosols from the tropics. By comparison, the Arctic region is more polluted with an order of magnitude higher OA levels compared to its analog of the SH (i.e. OA loadings ranging from 0.1 to 0.5 μg sm^{-3}). These concentrations are comparable to FT levels measured in the extratropical regions (25-55°N) of the NH. The equatorial marine regions (25°S-25°N) display the highest OA concentrations with a strong gradient between lower and upper troposphere. In the lower troposphere OA, concentrations are close to 1 μg sm^{-3}, and

https://doi.org/10.5194/acp-2019-773
Preprint. Discussion started: 20 September 2019

decrease down to 0.1 μg sm^{-3} at altitudes above 4km. The highest OA levels are associated with the African outflow over the southeastern Atlantic Ocean, which results from the transport of the biomass burning smoke from the sub-Saharan regions and increasing urban and industrial air pollution in southern West Africa (Flamant et al., 2018). Figure 2d shows that the Atlantic basin is often more polluted than the Pacific basin, not only because of the African biomass burning influence but also due to the contribution of anthropogenic pollution in the lower troposphere of the NH. It should be noted that while Asian pollution was intermittently sampled in the North Pacific Basin, no broad Asian outflow features were present in these two ATom deployments. Several-fold higher OA concentrations are found near the surface (below 1km) over the southern Pacific compared to that same location in the southern Atlantic, which could be indicative of the stronger emission of marine OA in the Pacific basin.

In addition to spatial gradients, a strong summer-to-winter contrast is observed in OA concentrations. Figure 2e shows the ratio between OA vertical profiles measured in the NH summer ATom-1 vs. in the NH winter ATom-2. The NH is more polluted during the NH summer due to the photochemical production of SOA, as well as biomass burning emissions, leading to the tripling of OA concentrations in the extratropical regions (25-80°N) on average regardless of altitude. The doubling of OA loading in the lower troposphere at the equator (25°S-25°N) in the NH summer (August, ATom-1) is strongly influenced by the biomass burning activity in the sub-Saharan African region as already mentioned above. Likewise, OA concentrations are found to be generally higher in the SH during the SH summer. These zonal trends are broadly similar to the ones described in Katich et al (2018) for BC.

4 Model-measurement comparisons

4.1 Evaluation of predicted OA concentrations

Prior to evaluating model performance in simulating OA, we have assessed the ATom models' ability to simulate sulfate aerosols. According to the model evaluation shown in Table S3, the predicted sulfate concentrations are generally within 40% of the measured values, which is comparable to the AMS measurement uncertainties. The only exception is found for the ECHAM6-HAM model, which overestimates sulfate aerosols by a factor of two. These results imply that most ATom models capture relatively well the overall sulfate burden. However, large root mean square error (RMSE > 0.4 μg sm^{-3} for ATom-1 and >

https://doi.org/10.5194/acp-2019-773
Preprint. Discussion started: 20 September 2019

0.2 μg sm^{-3} for ATom-2) is indicative of their limited skill in reproducing the observed variability in sulfate concentrations.

For OA, model evaluation metrics for the entire ATom-1 and ATom-2 campaigns are given in Table 2 for the eight ATom models and their ensemble, as well as the AeroCom-II ensemble. The results show that the normalized mean bias is substantially lower for the ATom model ensemble compared to AeroCom-II decreasing from 74% to 4% for ATom-1 and from 137% to 23% to ATom-2, which is within the measurement uncertainty range. The mean temporal correlations are substantially improved from 0.31 (0.38) for AeroCom-II to 0.66 (0.48) for ATom model ensemble during ATom-1 (ATom-2). However, results vary strongly among ATom models. Models using prescribed emissions of non-volatile SOA have the tendency to overestimate the OA concentrations (with ~35-60% overestimation for CESM2-SMP, ~70-100% for ECHAM6-HAM, and up to 150% for GC10-TOMAS during ATom-2), with the exception of the GEOS5-GOCART model that on the contrary underestimates OA concentrations by 5-25%. Models using the VBS parameterization from Pye et al. (2010) tend to underpredict the OA concentrations by 40-50% for GC12-REF and ~20-30% for CESM1-CARMA for ATom-1, most likely due to the excessive evaporation of the formed SOA in remote regions and low yields for anthropogenic SOA (Schroder et al., 2018; Shah et al., 2019). Models using the VBS parameterization from Hodzic et al. (2016) (CESM2-DYN and GC12-DYN) where OA is less volatile and also OA yields are corrected for wall losses in general show an improved agreement with observations especially for CESM2-DYN (within 5-30% for ATom-1 and 15-25% during ATom-2).

Figure 3 compares the average median ratios between modeled and observed OA concentrations for the ATom and AeroCom-II model ensembles for different regions (BB, MBL, FT, LS). The results show that the median ratio for the ATom model ensemble is close to unity in all regions. This is at least a factor of two improvement compared to AeroCom-II models, which were almost always biased high for the remote regions sampled in ATom. The model spread has also been reduced by a factor of 2-3 in all regions. This reduction in the ensemble spread may partially be explained by a smaller size of the ATom model ensemble, which also includes models that tend to have more focus on OA simulation. In order to explore this further, results for a subset of AeroCom-II models (using models related to those used in ATom) show only a slight reduction (~10%) in the model spread, with however some regional differences i.e. an improved

https://doi.org/10.5194/acp-2019-773
Preprint. Discussion started: 20 September 2019

agreement with observations in the MBL, but an increase in the model bias and spread in the LS (Figure S2).

4.2 Evaluation of predicted OA vertical distribution

Figure 4 compares the mean vertical profiles of OA measured during ATom-1 and -2 with the predictions of the model ensemble average based on the eight ATom models (Table 1) and 28 AeroCom-II models for the different latitudinal regions of the Pacific and Atlantic basins. Note that the use of a wide logarithmic scale may make the observed differences appear small, although they often reach factors of 2-10 and larger. For AeroCom-II, large latitudinal differences exist in the results with a better performance closer to source regions and large disagreement in the lower stratosphere and remote regions, as already suggested by the mission medians shown in Figure 3. The best AeroCom-II model performance is found over the equator in both basins, where the model ensemble captures within a factor of 2 the observed OA concentrations throughout the troposphere in the Pacific basin, and matches remarkably well the observations in the lower troposphere of the Atlantic basin that is heavily influenced by biomass burning emissions. Reasonable agreement is found for the OA vertical distribution over the NH Atlantic and Pacific oceans, especially in the lower troposphere (< 4 km). The largest model discrepancies (1-2 orders of magnitude) are found in the remote regions of the Southern Ocean and SH mid-latitudes during both seasons and basins. The model overestimation is also large over the NH mid-latitude Pacific basin in the upper troposphere. A spread of 2-3 orders of magnitude is observed around the ensemble average indicating a very large variability in individual model predictions. This evaluation of AeroCom-II models in remote regions is an extension of that performed at the surface for urban and remote stations by Tsigaridis et al. (2014) (as in that previous study, the data and model simulations compared are not synchronous in time). The tendency of the model ensemble to overpredict OA concentrations by a factor of 2 on average in the remote regions is consistent with the transition from the large underprediction in OA near the source region to a slight overprediction of OA in remote continental sites that was reported for most AeroCom-II models (Tsigaridis et al., 2014), and also observed for default parameterizations in other studies (Heald et al., 2011; Hodzic et al., 2016).

By comparison, the results of the ATom model ensemble show a much better agreement with observations. The model spread is still substantial, but mostly below a factor of 5. Figures S5 and S7 show OA vertical profiles for individual ATom models and the spread

https://doi.org/10.5194/acp-2019-773
Preprint. Discussion started: 20 September 2019

in their results. In most regions, the ATom model ensemble captures reasonably well both the absolute concentrations as well as the shape of the vertical profiles. In the biomass burning outflow and NH mid-latitude regions, the ATom ensemble average better captures the higher OA concentrations in the boundary layer and lower OA concentrations in the lower stratosphere than the AeroCom-II ensemble.

4.3 Oxidation level of organic aerosols (OA/OC ratios)

In addition to OA mass concentrations, we also evaluate the model's ability to simulate their degree of oxygenation, an indicator of their oxidation and aging (Aiken et al., 2008; Kroll et al., 2011). Ambient measurements of the oxidation level of organic particles are limited (Aiken et al., 2008, Canagaratna et al., 2015), and the ATom dataset provides the first global distribution of O/C and OA/OC ratios for the remote aerosol. The OA/OC ratio is an estimate of the average molecular weight of organic matter per carbon weight, and it mostly depends on the oxygen content (i.e. the O/C ratio), in the absence of significant concentrations of organonitrates and -sulfates. It is needed to compare measurements of organic aerosol mass (from e.g. AMS) with organic carbon measurements (from e.g. thermooptical methods). It is also needed to compare the various types of measurements to model concentrations, which are sometimes carried internally as OA and sometimes as OC. A low OA/OC ratio is indicative of freshly emitted OA from combustion (typically ~1.4), and its value increases with increased processing of organics in the atmosphere. Figure 5 shows that in the remote regions the bulk of measured OA/OC ratios during ATom-1 and -2 range between 2.2 and 2.5, and are larger than values of 2.1 ± 0.2 found in the polluted US continental outflow regions that were sampled during SEAC4RS, WINTER and DC3 field campaigns (Schroder et al., 2018). These values indicate that remote OA is highly oxidized and chemically processed.

Importantly, this ratio is also used to calculate the total OA mass concentration for models that provided their outputs in terms of organic carbon concentrations ($[OA]_i = [OC]_i \times OA/OC_{ratio}$). Most Models use a constant OA/OC ratio, but the value used varies substantially. OA/OC of 1.4 is used in ECHAM6-HAM, whereas 1.8 is used in GEOS5-GOCART and GC10-TOMAS simulations for both POA and SOA. Other models calculated directly SOA concentrations without applying this conversion (CESM1-CARMA, CESM2-SMP, CESM2-DYN, GC12-REF and GC12-DYN), but for POA used the ratio of 1.8 (CESM1-CARMA, CESM2-DYN) and 2.1 (GC12-REF and GC12-DYN). Most of the AeroCom-II models used the ratio of 1.4 for all primary and secondary OA (Tsigaridis et

https://doi.org/10.5194/acp-2019-773
Preprint. Discussion started: 20 September 2019

al., 2014). The comparison with measurements shows that the measured values are ~40% larger than those assumed in some of the ATom models, and 60-80% larger than used in AeroCom-II models. The comparison between the observed and predicted OA/OC vertical profiles (Fig. S3) shows that AeroCom-II models tend to generally underpredict this ratio, and do not capture its increase in remote regions. As a result, this underestimation of OA/OC ratios and the use of a constant value could substantially impact the comparisons of OA mass concentrations for several models considered in this study (ECHAM6-HAM, GEOS5-GOCART, CESM1-CARMA and GC10-TOMAS). If we correct for the underestimated OA/OC ratio using the ATom measured values of 2.2 (to be conservative) and compare to previously discussed biases in Table 2, the overprediction of the ECHAM6-HAM model is increased to ~110-160%, and that of GC10-TOMAS to 180% during ATom-2 while having ~15% bias in ATom-1, whereas GEOS5-GOCART results now overestimate up to 30% during ATom1, and perform much better during ATom-2.

These results demonstrate that current global chemistry-climate models use unrealistically low OA/OC ratios, which results in a large underestimate of the degree of oxidation of OA in remote regions. Inaccurate prediction of OA oxidation as it ages could impact not only the calculations of OA burden, but also its optical properties as the absorption of OA changes with its degree of oxidation (through the formation and destruction of brown carbon, Laskin et al., 2015, Forrister et al., 2015). However, models used in this study did not include these effects.

4.4 Contribution of primary vs. secondary OA

We further assess whether global models can adequately predict the relative contributions of primary and secondary OA. We strive to quantify these fractions with the most straightforward methods (with the fewest assumptions) for both models and measurements. POA concentrations were estimated from the BC measurements by using an emission ratio appropriate to the airmass origin (biomass burning vs. anthropogenic), using the f(BB) mass fraction from the PALMS single particle instrument (see Section 3.2). POA is assumed to be chemically inert, while in reality it can slowly be lost to the gas-phase by heterogeneous chemistry (e.g. George and Abbatt, 2010; Palm et al., 2018). Thus, the observation-based method provides an upper limit to the fraction of POA. The model/measurement comparison is only shown for the CESM and GEOS-Chem model variants, as other participating models do not separate or did not report their POA and SOA fractions. In all simulations, POA was treated as a chemically inert directly emitted

https://doi.org/10.5194/acp-2019-773
Preprint. Discussion started: 20 September 2019

primary aerosol species that only undergoes transport, transformation from hydrophobic to hydrophilic state with ageing (1-2 days typically), coagulation, and dry and wet deposition.

Figure 6 compares the vertical profiles of measurement-derived POA during ATom-1 and predicted by the CESM2-DYN model over clean remote regions of the Pacific basin and northern polar Atlantic that are not influenced by biomass burning. Comparisons for other models are similar (not shown). Observations show that POA is extremely small in remote regions, whereas the model predicts that about half of the OA is made of POA in those areas. Although the model reproduces quite well the measured total OA, it tends to severely overpredict the amount of POA and underpredict that of SOA over clean remote regions (with the two errors canceling each other when it comes to total OA). Over the biomass burning regions (not shown here) it can be difficult to directly quantify POA and SOA with this method, as total OA remains about constant, while POA decreases with aging and SOA increases (Cubison et al., 2011; Jolleys et al., 2015; Hodshire et al., 2019b). However, given this evolution the method used here would lead to an overestimate of POA for this reason.

A more general comparison is made in Figure 7, using the frequency distributions of the measured and simulated fraction of POA/OA, for the free troposphere only (Figure S8 shows the corresponding cumulative distributions). Observations indicate that most remote FT airmasses contain less than 10% POA, except for biomass burning plumes that are considered mostly primary. A slightly higher proportion of POA is seen in ATom-2, which is consistent with a slower photochemical production of SOA during NH winter. These results indicate that the remote OA is consistently dominated by SOA regardless of the season and location. The comparison with models reveals a very large discrepancy in the predicted vs. measured POA vs. SOA contributions. Models have a general tendency to severely overpredict the fraction of POA and underpredict that of SOA, displaying a much wider frequency distribution than the measurements (as also shown for POA and SOA vertical profiles for individual models on Figures S5 and S7). In GC12-REF, CESM2-DYN and CESM1-CARMA (without improved in-cloud removal) predictions for ATom-1, more than a half of the remote OA is POA, while that is very rarely observed in the free troposphere (possibly only during strong biomass burning events). Most models fail to reproduce the overwhelming dominance of SOA that is seen in the measurements during ATom-1, while the discrepancies are less severe during NH winter (ATom-2).

https://doi.org/10.5194/acp-2019-773
Preprint. Discussion started: 20 September 2019

These seasonal differences suggest that model errors could be partially due to inefficient production of SOA, although removal errors also probably play a major role (see next section).

The differences are so large that they are pretty insensitive to details of the POA estimation method from the measurements. As Figure S9 illustrates, the choice of FF_{ratio} has very little impact on the overall distribution of POA. On the other hand, while the BB_{ratio} does impact the overall distribution of POA, it mostly affects the points in the vicinity of the large Atlantic plumes. Since the POA/BC ratio in those plumes is fairly low, (see Section 3.2), using a very large BB_{ratio} mostly leads to an increase of the fraction of the points where POA > 100%. While the large range of published BB_{ratio} for different sources precludes a more accurate estimation by our method, for the purposes of the comparison with the model results we emphasize that even using the largest BB_{ratio}, f(SOA) is still significantly larger in the ATom dataset that in any of the models.

A comparison between simulations that have the same treatment of POA, and only differ in their chemistry and removal of SOA (e.g. CESM2-SMP vs. CESM2-DYN; GC12-REF vs. GC12-DYN) indicate that a more complex SOA treatment does not always result in a more accurate simulation of the primary/secondary character of OA, a result that was also found in the AeroCom-II multi-model intercomparison (Tsigaridis et al., 2014).

4.5 Sensitivity to OA formation and removal

In this section, we further investigate some of the possible reasons for the incorrect model predictions of the relative contributions of POA and SOA in remote regions. Given the tendency of models to underestimate OA close to anthropogenic source regions and overestimate OA downwind in past studies (e.g. Heald et al., 2011; Tsigaridis et al., 2014; Hodzic et al., 2016), in this section we investigate the sensitivity of OA to increasing sources and increasing removals. We have performed two additional model simulations to test the sensitivity of the POA/SOA fractions to uncertainties in the representation of (i) wet scavenging, based on the CESM1-CARMA simulations in which we have removed the improvements in the aerosol removal by the convective updrafts (Yu et al., 2019); and of (ii) SOA formation based on the GC12-REF simulations in which we have replaced the SOA formation VBS mechanism (Pye et al., 2010) by an updated VBS mechanism that uses chamber wall-loss corrected SOA yields (Hodzic et al., 2016, same formation scheme that is used in GC12-DYN and CESM2-DYN runs, but with removals kept identical to GC12-REF). The results of these two sensitivity simulations are displayed on Figure 8,

https://doi.org/10.5194/acp-2019-773
Preprint. Discussion started: 20 September 2019

which shows measured and predicted mass concentrations of OA, POA, SOA and sulfate for ATom-1 as a function of the number of days since the air mass was processed through convection. One should keep in mind that this is an averaged plot that included airmasses from various regions and altitudes, and not a Lagrangian plot following the same airmass.

Sensitivity to in-cloud scavenging in convective clouds. Inefficient wet removal of primary OA could contribute to the POA overprediction in global models, especially in the tropics. Previous global model studies have reported two to three orders of magnitude overestimation of primary carbonaceous species such as BC in the free troposphere when the removal in the convective updrafts was not included (e.g. Schwarz et al., 2013, Yu et al., 2019). A strong reduction due to convective removal is also expected for POA concentrations, as POA is a primary species co-emitted with BC at the surface and internally mixed with it (Lee et al., 2015), and that is typically coated by secondary inorganics and organics over short timescales (Petters et al., 2006; Jiang et al., 2010; Wang et al., 2010). Figures 7a and 8 compare the simulations of CESM1-CARMA with and without improved convective in-cloud scavenging during ATom-1. The improved in-cloud scavenging scheme considers aerosol activation into cloud droplets from entrained air above the cloud base, which is more realistic and results in a more efficient removal of aerosols in the upper troposphere by convection. E.g. a two order of magnitude reduction in BC in the upper FT was reported by Yu et al. (2019), resulting in much improved agreement with observations. Similar results were observed for sea salt aerosols in Murphy et al. (2019). Figure 8 shows that all submicron aerosol species simulated in CESM1-CARMA are strongly impacted by the in-cloud removal above the cloud base. POA concentrations are reduced by an order of magnitude while sulfate is reduced by 30% leading in both cases to a much-improved agreement with observations. SOA is reduced by ~30% as well, which leads to an underprediction of measured SOA concentrations. The overall impact on OA concentrations is a significant reduction, which leads to ~20% underestimation of OA in the aged remote air during ATom-1.

For the CESM2-DYN model that does not have improved in-cloud removal, the reasonable agreement (within 20%) with the observed OA concentrations thus results from coincidental error compensation between the overpredicted POA and underpredicted SOA. The prescribed SOA formation and the artificial 50% adjustment of SOA emissions based on Liu et al. (2012) leads to an overestimation of observed SOA in aged remote airmasses.

https://doi.org/10.5194/acp-2019-773
Preprint. Discussion started: 20 September 2019

Sensitivity to SOA formation. In addition, we have also tested the sensitivity of the OA composition to the choice of the SOA formation mechanism. Figure 8 compares the results of the GC12-REF model that uses SOA formation yields derived from traditional chamber experiments (Pye et al., 2010) and those corrected for loses of organic vapors onto chamber walls as proposed in Hodzic et al. (2016). Previous studies have reported that chamber wall losses could lead up to a factor of 4 underprediction of formed SOA (Zhang et al., 2014; Krechmer et al., 2016). The comparison shows a factor of 3 increase in SOA concentrations when the updated SOA formation is considered leading to a much better agreement with the observed SOA as well as the observed total OA. GC12-REF predicts well the amount of POA and overpredicts somewhat the amount of sulfate aerosols, which is expected as it already includes the improved aerosol removal in convective updrafts (Wang et al., 2014). Figure S6 also shows that POA vertical distribution is well captured in GEOS-Chem in most regions, except over the polar north Pacific. It should be noted that these results are consistent with the POA/OA frequency distribution shown in Figure 7 (e.g. GC12-REF POA/OA is shifted rightward compared to observations in Figure 7, which is consistent with the fact that POA is about the right amount, and OA is underpredicted in Figure 8).

These sensitivity simulations suggest that a stronger convective removal of POA and a stronger production of SOA might be needed to correctly represent not only the total OA concentrations but also its primary and secondary nature in remote free troposphere and remote ocean regions. Accurate predictions of the OA concentration, composition, and source contributions for the right reasons are key for accurately predicting their lifecycle and radiative impacts. Only when there is confidence that the sources are accurately predicted, we can have confidence in OA predictions for pre-industrial and future conditions, as well as to evaluate PM mitigation strategies.

4.6 OA and sulfate relative contributions in FT

Finally, we assess the model ability to predict relative amounts of OA and sulfate in the free troposphere where they are the two major constituents of the submicron aerosol (Figure 2b). Accurate predictions of their relative contributions are crucial to determine the hygroscopicity of the submicron aerosol, and its ability to serve as a cloud condensation nuclei (CCN) in the remote free troposphere (Carslaw et al., 2013; Brock et al., 2016).

Figure 9a compares the average measured relative fractions of sulfate (36%) and carbonaceous aerosols (OA=59% and BC=5%) in the FT with those predicted by

https://doi.org/10.5194/acp-2019-773
Preprint. Discussion started: 20 September 2019

individual models during ATom-1. The CESM2 models best reproduce the observed relative contributions, with a slight underestimation of OA (57% instead of 59%) for CESM2-DYN, and a slight overestimation of OA (63% instead of 59%) for CESM2-SMP. GEOS5-GOCART has 15% more OA relative to sulfate than observed. All other models underestimate both OA and BC relative fractions. For instance, in GC12-REF and -DYN, both the BC and OA fractions are ~40% (relative) lower than observed.

Figure 9b shows the frequency distribution of observed and predicted fractions of OA relative to sulfate during ATom-1 and -2 in the free troposphere. Most models fail to reproduce the relatively uniform nature of the observed distributions during ATom-1, with typically narrower model shapes around a preferred ratio. The NH summer measurements indicate that OA > sulfate in ~55% of the samples (consistent with Fig. 2b), while models generally tend to underestimate the relative OA contribution. In particular, GEOS-Chem and ECHAM6-HAM tend to overestimate the relative contribution of sulfate. A better agreement is found for GEOS5-GOCART, CESM1-CARMA and CESM2-DYN, which follow more closely the shape of the observed distribution. The comparisons also suggest that the more complex SOA treatment of SOA formation and removal proposed by Hodzic et al. (2016) in the same host model leads to an improved agreement with observations (e.g. CESM2-DYN vs. CESM2-SMP; GC12-DYN vs. GC12-REF). It should be noted that CESM2-SMP uses fixed SOA yields that were increased by 50% as suggested by Liu et al. (2012), leading to an overestimation of the relative contribution of OA compared to that of sulfate in the free troposphere. During the NH winter (ATom-2), measurements show a somewhat higher proportion of sulfate aerosols (vs. ATom-1), which is consistent with a slower production of SOA in the NH during winter and a reduced influence of biomass burning. Similar conclusions are found for the evaluation of different models. It is worth mentioning that the comparison performed for the whole ATom-1 and 2 dataset (not shown) leads to similar results with even slightly stronger overestimation of the sulfate relative contribution compared to OA.

The discrepancies between the observed and predicted composition of submicron aerosol over remote regions can be quite large for other constituents as well. Figure 10 shows the comparison of measured and predicted composition of the submicron aerosol over the Southern Ocean (during the NH winter) where the disagreement in simulated sea salt, nitrates, ammonium, and MSA often exceeds the contribution of OA. While the observations show a more uniform distribution of non-marine aerosol with higher values

https://doi.org/10.5194/acp-2019-773
Preprint. Discussion started: 20 September 2019

in the mid and upper troposphere, respectively, most models tend to simulate highest fractions of sulfate and OA towards the tropopause. This may also be explained by the uncertainties in modeled wet removal of aerosol that has been discussed above.

5 Conclusions and implications

Our understanding and representation in global models of the lifecycle of the OA remain highly uncertain, especially in remote regions where constraints from measurements have been very sparse. We have performed a systematic evaluation of the performance of eight global chemistry climate models and of 28 AeroCom-II models in simulating the latitudinal and vertical distribution of OA and its composition in the remote regions of the Atlantic and Pacific marine boundary layer, free troposphere and lower stratosphere, using the unique measurements from the ATom campaign. Our simulations are conducted for both ATom-1 and ATom-2 deployments that took place in August 2016 and February 2017, respectively. The main conclusions of the comparison are as follows:

- The AeroCom-II ensemble average tends to be biased high by a factor of 2-5 in comparison to measured vertical OA profiles in the remote atmosphere during both NH summer and NH winter. The ensemble spread increases from a factor of 40 in the NH source regions to a factor of 1000 in remote regions of the Southern Ocean. The evaluation of AeroCom-II models in the remote regions provides an extension of the previous evaluation with continental ground data by Tsigaridis et al. (2014). We note that the data from the AeroCom-II models were based on monthly mean values from a different simulated year than the ATom campaigns; however, the consistent model biases are strong enough that we would not expect our conclusions to change for a different modeled year.
- The results of the ATom model ensemble used in this work show a much better agreement with the OA observations in all regions and reduced model variability. However, some of the agreement is for the wrong reasons, as most models severely overestimate the contribution of POA and underestimate the contribution of SOA to total OA. Sensitivity simulations indicate that the POA overestimate in CESM could be due to an inadequate representation of primary aerosol removal by convective clouds, (additional convective removal per Yu et al. (2019) in CESM1-CARMA led to a better agreement with observations). Most models have insufficient production of SOA, and

https://doi.org/10.5194/acp-2019-773
Preprint. Discussion started: 20 September 2019

sensitivity studies indicate that a stronger production of SOA is needed to capture the measured concentrations. The photochemical ageing of POA which was not considered here (unlike for SOA) could also contribute to the model overestimation. The compensation between errors in POA and SOA in remote regions is however a recurring issue in OA modeling (de Gouw and Jimenez, 2009). For instance, it was found in the urban outflow regions such as Mexico City during MILAGRO 2006 field campaign (Fast et al., 2009; Hodzic et al., 2009); Paris during MEGAPOLI 2009 (Zhang et al., 2013); the Los Angeles area during CalNex-2010 (Baker et al., 2015; Woody et al., 2016); the NE US outflow during WINTER 2015 (Schroder et al., 2018; Shah et al., 2019).

- Additional errors in simulated OA concentrations can arise from the use of too low OA/OC ratios when model results (often calculated as OC) are converted to OA for comparison with measurements. We note that OA is the most atmospherically-relevant quantity, while OC is an operational quantity, partially a relic from a period in which only OC could be separately quantified (although also of some use for carbon budget studies). It should also be noted that most emission inventories still use OC as the primary variable, which is why the use of accurate OA/OC ratios is still key for all models. We show that the OA/OC ratio used in most models is too low compared to measured values that range mostly from 2.2 to 2.5, resulting in errors in OA mass of ~70% for AeroCom-II models and ~30% for current models that use organic carbon to track OA mass. Remote OA is thus highly oxidized and chemically processed. These results demonstrate that current global chemistry-climate models underestimate the degree of oxidation of OA in remote regions and need to consider further chemical ageing of OA, which could impact the calculations of its burden, and optical and hygroscopic properties.
- The results also show that in most models (except CESM2) the predicted OA contribution to the total submicron aerosol is underestimated relative to sulfate in the remote FT where OA and sulfate are the dominant submicron aerosols (important for climate). Accurate predictions of composition of submicron particles remains challenging in remote regions and should be the topic of future studies.

Key implications of our results are: (i) Model errors on the relative contribution of POA and SOA to OA reduce our confidence on the ability to simulate radiative forcing over time or OA health impacts; (ii) Model errors for the relative contributions of sulfate and organics to the submicron aerosol in the free troposphere could lead to errors in the predicted CCN

or radiative forcing of aerosols as inorganics are more hygroscopic than OA; (iii) the OA system seems to be more dynamic with a need for an enhanced removal of primary OA, and a stronger production of secondary OA in global models to provide a better agreement with observations.

Acknowledgements. The authors want to thank the ATom leadership team and the NASA logistics and flight crew for their contributions to the success of ATom. Authors acknowledge Dr. Rebecca Buchholz (NCAR) for providing the emissions used for the CESM2 simulations. The ATOM measurements and analyses were supported by NASA grants NNX15AH33A, NNX15AJ23G, and 80NSSC19K0124. AH was supported by the National Center for Atmospheric Research, which is operated by the University Corporation for Atmospheric Research on behalf of the National Science Foundation. JRP and JKK were supported by the US Department of Energy's Atmospheric System Research, an Office of Science, Office of Biological and Environmental Research program, under grant no. DE-SC0019000. This project has received support from the European Research Council under the European Union's Horizon 2020 research and innovation programme (grant agreement No. 819169), and from EPA STAR grant 83587701-0. This manuscript has not been reviewed by EPA, and no endorsement should be inferred. We would like to acknowledge high-performance computing support from Cheyenne provided by NCAR's Computational and Information Systems Laboratory.

Code/Data availability: All data can be obtained from the ATom website: https://doi.org/10.3334/ORNLDAAC/1581.

Author contribution: Hodzic A. performed the analysis of the models/measurements comparisons, performed certain model simulations, and wrote most of the manuscript. Campuzano-Jost P. performed the analysis of the models/measurements comparisons, performed AMS measurements, and contributed to the manuscript. Jimenez J. contributed to the interpretation of the results and the elaboration of the manuscript. All other authors provided either measurements or model outputs that are used in the paper, and feedback on the manuscript.

References

Aiken, A.C., P.F. DeCarlo, J.H. Kroll, D.R. Worsnop, J.A. Huffman, K. Docherty, I.M. Ulbrich, C. Mohr, J.R. Kimmel, D. Sueper, Q. Zhang, Y. Sun, A. Trimborn, M. Northway, P.J. Ziemann, M.R. Canagaratna, T.B. Onasch, R. Alfarra, A.S.H. Prevot, J. Dommen, J.

Duplissy, A. Metzger, U. Baltensperger, and J.L. Jimenez. O/C and OM/OC Ratios of Primary, Secondary, and Ambient Organic Aerosols with High Resolution Time-of-Flight Aerosol Mass Spectrometry Environmental Science & Technology, 42, 4478–4485, doi: 10.1021/es703009q, 2008.

Andreae, M. O.: Emission of trace gases and aerosols from biomass burning – An updated assessment, Atmos. Chem. Phys. Discuss., 1–27, doi:10.5194/acp-2019-303, 2019.

Bey, I., Jacob, D. J., Yantosca, R. M., and Logan, J. A.: Global modeling of tropospheric chemistry with assimilated meteorology: model description and evaluation, J Geophys. Res., 106, 23073–23095, 2011.

Baker, K. R., Carlton, A. G., Kleindienst, T. E., Offenberg, J. H., Beaver, M. R., Gentner, D. R., Goldstein, A. H., Hayes, P. L., Jimenez, J. L., Gilman, J. B., de Gouw, J. A., Woody, M. C., Pye, H. O. T., Kelly, J. T., Lewandowski, M., Jaoui, M., Stevens, P. S., Brune, W. H., Lin, Y.-H., Rubitschun, C. L., and Surratt, J. D.: Gas and aerosol carbon in California: comparison of measurements and model predictions in Pasadena and Bakersfield, Atmos. Chem. Phys., 15, 5243-5258, https://doi.org/10.5194/acp-15-5243-2015, 2015.

Bian, H., Froyd, K., Murphy, D. M., Dibb, J., Chin, M., Colarco, P. R., Darmenov, A., da Silva, A., Kucsera, T. L., Schill, G., Yu, H., Bui, P., Dollner, M., Weinzierl, B., and Smirnov, A.: Observationally constrained analysis of sea salt aerosol in the marine atmosphere, Atmos. Chem. Phys. Discuss., https://doi.org/10.5194/acp-2019-18, 2019.

Bian, H., Chin, M., Hauglustaine, D. A., Schulz, M., Myhre, G., Bauer, S. E., Lund, M. T., Karydis, V. A., Kucsera, T. L., Pan, X., Pozzer, A., Skeie, R. B., Steenrod, S. D., Sudo, K., Tsigaridis, K., Tsimpidi, A. P., and Tsyro, S. G.: Investigation of global nitrate from the AeroCom Phase III experiment, Atmos. Chem. Phys., 17, 12911-12940, https://doi.org/10.5194/acp-17-12911-2017, 2017.

Boucher, O., D. Randall, P. Artaxo, C. Bretherton, G. Feingold, P. Forster, V.-M. Kerminen, Y. Kondo, H. Liao, U. Lohmann, P. Rasch, S.K. Satheesh, S. Sherwood, B. Stevens and X.Y. Zhang: Clouds and Aerosols. In: Climate Change 2013: The Physical Science Basis. Contribution of Working Group I to the Fifth Assessment Report of the Intergovernmental Panel on Climate Change [Stocker, T.F., D. Qin, G.-K. Plattner, M. Tignor, S.K. Allen, J. Boschung, A. Nauels, Y. Xia, V. Bex and P.M. Midgley (eds.)]. Cambridge University Press, Cambridge, United Kingdom and New York, NY, USA, 2013.

https://doi.org/10.5194/acp-2019-773
Preprint. Discussion started: 20 September 2019

Bowman, K. P.: Large-scale isentropic mixing properties of the Antarctic polar vortex from analyzed winds. J. Geophys. Res., 98 (D12), 23 013–23 027, 1993.

Brock, C. A., Wagner, N. L., Anderson, B. E., Attwood, A. R., Beyersdorf, A., Campuzano-Jost, P., Carlton, A. G., Day, D. A., Diskin, G. S., Gordon, T. D., Jimenez, J. L., Lack, D. A., Liao, J., Markovic, M. Z., Middlebrook, A. M., Ng, N. L., Perring, A. E., Richardson, M. S., Schwarz, J. P., Washenfelder, R. A., Welti, A., Xu, L., Ziemba, L. D., and Murphy, D. M.: Aerosol optical properties in the southeastern United States in summer – Part 1: Hygroscopic growth, Atmos. Chem. Phys., 16, 4987-5007, https://doi.org/10.5194/acp-16-4987-2016, 2016.

Brock, C. A., Williamson, C., Kupc, A., Froyd, K. D., Erdesz, F., Wagner, N., Richardson, M., Schwarz, J. P., Gao, R.-S., Katich, J. M., Campuzano-Jost, P., Nault, B. A., Schroder, J. C., Jimenez, J. L., Weinzierl, B., Dollner, M., Bui, T. and Murphy, D. M.: Aerosol size distributions during the Atmospheric Tomography Mission (ATom): methods, uncertainties, and data products, Atmos. Meas. Tech., 12(6), 3081–3099, doi:10.5194/amt-12-3081-2019, 2019.

Canagaratna, M. R., Jayne, J. T., Jimenez, J. L., Allan, J. D., Alfarra, M. R., Zhang, Q., Onasch, T. B., Drewnick, F., Coe, H., Middlebrook, A. M., Delia, A., Williams, L. R., Trimborn, A. M., Northway, M. J., DeCarlo, P. F., Kolb, C. E., Davidovits, P., and Worsnop, D. R.: Chemical and microphysical characterization of ambient aerosols with the Aerodyne Aerosol Mass Spectrometer, Mass Spectrom. Rev., 26, 185–222, https://doi.org/10.1002/mas.20115, 2007.

Canagaratna, M. R., Jimenez, J. L., Kroll, J. H., Chen, Q., Kessler, S. H., Massoli, P., Hildebrandt Ruiz, L., Fortner, E., Williams, L. R., Wilson, K. R., Surratt, J. D., Donahue, N. M., Jayne, J. T., and Worsnop, D. R.: Elemental ratio measurements of organic compounds using aerosol mass spectrometry: characterization, improved calibration, and implications, Atmos. Chem. Phys., 15, 253-272, https://doi.org/10.5194/acp-15-253-2015, 2015.

Carslaw, K. S., Lee, L. a, Reddington, C. L., Pringle, K. J., Rap, A., Forster, P. M., Mann, G. W., Spracklen, D. V, Woodhouse, M. T., Regayre, L. a and Pierce, J. R.: Large contribution of natural aerosols to uncertainty in indirect forcing., Nature, 503(7474), 67–71, doi:10.1038/nature12674, 2013.

Colarco, P., da Silva, A., Chin, M., and Diehl, T.: Online simulations of global aerosol distributions in the NASA GEOS-4 model and comparisons to satellite and ground based aerosol optical depth, J. Geophys. Res., 115, D14207, doi:10.1029/2009JD012820, 2010.

Cubison, M. J., Ortega, A. M., Hayes, P. L., Farmer, D. K., Day, D., Lechner, M. J., Brune, W. H., Apel, E., Diskin, G. S., Fisher, J. A., Fuelberg, H. E., Hecobian, A., Knapp, D. J., Mikoviny, T., Riemer, D., Sachse, G. W., Sessions, W., Weber, R. J., Weinheimer, A. J., Wisthaler, A., and Jimenez, J. L.: Effects of aging on organic aerosol from open biomass burning smoke in aircraft and laboratory studies, Atmos. Chem. Phys., 11, 12049-12064, https://doi.org/10.5194/acp-11-12049-2011, 2011.

DeCarlo, P., Slowik, J., Worsnop, D., Davidovits, P., Jimenez, J., Stainken, K., Williams, L., Jayne, J., Kolb, C. and Rudich, Y.: Particle Morphology and Density Characterization by Combined Mobility and Aerodynamic Diameter Measurements. Part 1: Theory, Aerosol Sci. Technol., 38(12), 1185–1205, doi:10.1080/027868290903907, 2004.

DeCarlo, P. F., Kimmel, J. R., Trimborn, A., Northway, M. J., Jayne, J. T., Aiken, A. C., Gonin, M., Fuhrer, K., Horvath, T., Docherty, K. S., Worsnop, D. R., and Jimenez, J. L.: Field-Deployable, High-Resolution, Time-of-Flight Aerosol Mass Spectrometer, Anal. Chem., 78, 8281–8289, https://doi.org/10.1021/ac061249n, 2006.

de Gouw, J., and J.L. Jimenez. Organic Aerosols in the Earth's Atmosphere. Environmental Science & Technology, 43, 7614–7618, 2009. DOI: 10.1021/es9006004

Dentener, F., Kinne, S., Bond, T., Boucher, O., Cofala, J., Generoso, S., Ginoux, P., Gong, S., Hoelzemann, J. J., Ito, A., Marelli, L., Penner, J. E., Putaud, J.-P., Textor, C., Schulz, M., van der Werf, G. R., and Wilson, J.: Emissions of primary aerosol and precursor gases in the years 2000 and 1750 prescribed data-sets for AeroCom, Atmospheric Chemistry and Physics, 6, 4321–4344, https://doi.org/10.5194/acp- 6-4321-2006, https://www.atmos-chem-phys.net/6/4321/2006/, 2006.

Drewnick, F., Hings, S. S., Alfarra, M. R., Prevot, A. S. H. and Borrmann, S.: Aerosol quantification with the Aerodyne Aerosol Mass Spectrometer: detection limits and ionizer background effects, Atmos. Meas. Tech., 2(1), 33–46, 2009.

Emmons, L. K., Orlando, J. J., Tyndall, G., Schwantes, R. H., Kinnison, D. E., Marsh, D. R., Mills, M. J., Tilmes, S., and Lamarque, J.-F.: The MOZART Chemistry Mechanism in the Community Earth System Model version 2 (CESM2), to be Submitted to J. Adv. Modeling Earth Systems, 2019.

Fast, J., Aiken, A. C., Allan, J., Alexander, L., Campos, T., Canagaratna, M. R., Chapman, E., DeCarlo, P. F., de Foy, B., Gaffney, J., de Gouw, J., Doran, J. C., Emmons, L., Hodzic, A., Herndon, S. C., Huey, G., Jayne, J. T., Jimenez, J. L., Kleinman, L., Kuster, W., Marley, N., Russell, L., Ochoa, C., Onasch, T. B., Pekour, M., Song, C., Ulbrich, I. M., Warneke, C., Welsh-Bon, D., Wiedinmyer, C., Worsnop, D. R., Yu, X.-Y., and Zaveri, R.: Evaluating simulated primary anthropogenic and biomass burning organic aerosols during MILAGRO: implications for assessing treatments of secondary organic aerosols, Atmos. Chem. Phys., 9, 6191-6215, https://doi.org/10.5194/acp-9-6191-2009, 2009.

Flamant, C., Knippertz, P., Fink, A. H., Akpo, A., Brooks, B., Chiu, C. J., Coe, H., Danuor, S., Evans, M., Jegede, O., Kalthoff, N., Konaré, A., Liousse, C., Lohou, F., Mari, C., Schlager, H., Schwarzenboeck, A., Adler, B., Amekudzi, L., Aryee, J., Ayoola, M., Batenburg, A. M., Bessardon, G., Borrmann, S., Brito, J., Bower, K., Burnet, F., Catoire, V., Colomb, A., Den- jean, C., Fosu-Amankwah, K., Hill, P. G., Lee, J., Lothon, M., Maranan, M., Marsham, J., Meynadier, R., Ngamini, J.-B., Rosenberg, P., Sauer, D., Smith, V., Stratmann, G., Taylor, J. W., Voigt, C., and Yoboué, V.: The Dynamics-Aerosol-Chemistry- Cloud Interactions in West Africa field campaign: Overview and research highlights, B. Am. Meteorol. Soc., 99, 83–104, https://doi.org/10.1175/BAMS-D-16-0256.1, 2018.

Forrister, H., Liu, J., Scheuer, E., Dibb, J., Ziemba, L., Thornhill, K. L., Anderson, B., Diskin, G., Perring, A. E., Schwarz, J. P., Campuzano-Jost, P., Day, D. A., Palm, B. B., Jimenez, J. L., Nenes, A. and Weber, R. J.: Evolution of brown carbon in wildfire plumes, Geophys. Res. Lett., 42(11), doi:10.1002/2015GL063897, 2015.

Fountoukis, C. and Nenes, A.: ISORROPIA II : a computationally efficient thermodynamic equilibrium model for K+-Ca2+-Mg2+-Na+-SO42--NO3--Cl--H2O aerosols, Atmos. Chem. Phys., 7, 4639–4659, 2007.

Froyd, K. D., Murphy, D. M., Brock, C. A., Campuzano-Jost, P., Dibb, J. E., Jimenez, J.-L., Kupc, A., Middlebrook, A. M., Schill, G. P., Thornhill, K. L., Williamson, C. J., Wilson, J. C., and Ziemba, L. D.: A new method to quantify mineral dust and other aerosol species from aircraft platforms using single particle mass spectrometry, Atmos. Meas. Tech. Discuss., https://doi.org/10.5194/amt-2019-165, in review, 2019.

George, I. J. and Abbatt, J. P. D.: Heterogeneous oxidation of atmospheric aerosol particles by gas-phase radicals, Nature Chemistry, 2, 713–722, 2010.

Gettelman, A., Mills, M. J., Kinnison, D. e., Garcia, R. R., Smith, A. K., Marsh, D. R., Tilmes, S., Vitt, F., Bardeen, C. G., McInerny, J., Liu, H.-L., Solomon, S. C., Polvani, L. M., Emmons, L. K., Lamarque, J.-F., Richter, J. H., Glanville, A. S., Bacmeister, J. T., Phillips, A. S., Neale, R. B., Simpson, I. R., DuVivier, A. K., Hodzic, A., Randel, W. J.: The Whole Atmosphere Community Climate Model Version 6 (WACCM6), J. of Geophys. Res., in review, 2019.

Giglio, L., Randerson, J. T. and Werf, G. R.: Analysis of daily, monthly, and annual burned area using the fourth-generation global fire emissions database (GFED4), J. Geophys. Res. Biogeosciences, 118, 317–328, 2013.

Guo H, Campuzano-Jost, P, Nault, B.A. Schroder, J.C. Day, D.A. Williamson, C, Kupc, A, Brock, C.A. Froyd, K. Jimenez, J.L.: Evaluating the Aerosol Mass Spectrometer Quantified Submicron Aerosol Volume during the Atmospheric Tomography Mission (ATom), to be submitted to AMTD, 2019.

Guenther, A. B., Jiang, X., Heald, C. L., Sakulyanontvittaya, T., Duhl, T., Emmons, L. K., and Wang, X.: The Model of Emissions of Gases and Aerosols from Nature version 2.1 (MEGAN2.1): an extended and updated framework for modeling biogenic emissions, Geosci. Model Dev., 5, 1471–1492, https://doi.org/10.5194/gmd-5-1471-2012, https://www.geosci-model-dev.net/5/1471/2012/, 2012.

Hayes, P. L., Carlton, A. G., Baker, K. R., Ahmadov, R., Washenfelder, R. A., Alvarez, S., Rappenglück, B., Gilman, J. B., Kuster, W. C., de Gouw, J. A., Zotter, P., Prévôt, A. S. H., Szidat, S., Kleindienst, T. E., Offenberg, J. H., Ma, P. K., and Jimenez, J. L.: Modeling the formation and aging of secondary organic aerosols in Los Angeles during CalNex 2010, Atmos. Chem. Phys., 15, 5773-5801, https://doi.org/10.5194/acp-15-5773-2015, 2015.

Hallquist, M., Wenger, J. C., Baltensperger, U., Rudich, Y., Simpson, D., Claeys, M., Dommen, J., Donahue, N. M., George, C., Goldstein, A. H., Hamilton, J. F., Herrmann, H., Hoffmann, T., Iinuma, Y., Jang, M., Jenkin, M. E., Jimenez, J. L., Kiendler-Scharr, A., Maenhaut, W., McFiggans, G., Mentel, Th. F., Monod, A., Prévôt, A. S. H., Seinfeld, J. H., Surratt, J. D., Szmigielski, R., and Wildt, J.: The formation, properties and impact of secondary organic aerosol: current and emerging issues, Atmos. Chem. Phys., 9, 5155-5236, https://doi.org/10.5194/acp-9-5155-2009, 2009.

Heald, C. L., Coe, H., Jimenez, J. L., Weber, R. J., Bahreini, R., Middlebrook, A. M., Russell, L. M., Jolleys, M., Fu, T.-M., Al- lan, J. D., Bower, K. N., Capes, G., Crosier, J.,

Morgan, W. T., Robinson, N. H., Williams, P. I., Cubison, M. J., DeCarlo, P. F., and Dunlea, E. J.: Exploring the vertical profile of atmospheric organic aerosol: comparing 17 aircraft field campaigns with a global model, Atmos. Chem. Phys., 11, 12673–12696, doi:10.5194/acp-11-12673-2011, 2011.

Hodshire, A. L., Campuzano-Jost, P., Kodros, J. K., Croft, B., Nault, B. A., Schroder, J. C., Jimenez, J. L. and Pierce, J. R.: The potential role of methanesulfonic acid (MSA) in aerosol formation and growth and the associated radiative forcings, Atmos. Chem. Phys., 19(5), 3137–3160, doi:10.5194/acp-19-3137-2019, 2019a.

Hodshire, A., A. Akherati, M. Alvarado, B. Brown-Steiner, S. Jathar, J.L. Jimenez, S. Kreidenweis, C. Lonsdale, T. Onasch, A. Ortega, J. Pierce. Aging Effects on Biomass Burning Aerosol Mass and Composition: A Critical Review of Field and Laboratory Studies. Environ. Sci. Technol., submitted, 2019b.

Hodzic, A., Jimenez, J. L., Madronich, S., Aiken, A. C., Bessagnet, B., Curci, G., Fast, J., Lamarque, J.-F., Onasch, T. B., Roux, G., Schauer, J. J., Stone, E. A., and Ulbrich, I. M.: Modeling organic aerosols during MILAGRO: importance of biogenic secondary organic aerosols, Atmos. Chem. Phys., 9, 6949-6981, https://doi.org/10.5194/acp-9-6949-2009, 2009.

Hodzic, A., Aumont, B., Knote, C., Lee-Taylor, J., Madronich, S., and Tyndall, G.: Volatility dependence of Henry's law constants of condensable organics: Application to estimate depositional loss of secondary organic aerosols, Geophys. Res. Lett., 41, 4795–4804, doi:10.1002/2014GL060649, 2014.

Hodzic, A., Madronich, S., Kasibhatla, P. S., Tyndall, G., Aumont, B., Jimenez, J. L., Lee-Taylor, J., and Orlando, J.: Organic photolysis reactions in tropospheric aerosols: effect on secondary organic aerosol formation and lifetime, Atmos. Chem. Phys., 15, 9253-9269, https://doi.org/10.5194/acp-15-9253-2015, 2015.

Hodzic, A., Kasibhatla, P. S., Jo, D. S., Cappa, C. D., Jimenez, J. L., Madronich, S., and Park, R. J.: Rethinking the global secondary organic aerosol (SOA) budget: stronger production, faster removal, shorter lifetime, Atmos. Chem. Phys., 16, 7917-7941, https://doi.org/10.5194/acp-16-7917-2016, 2016.

Huang, K., Fu, J. S., Prikhodko, V. Y., Storey, J. M., Romanov, A., Hodson, E. L., Cresko, J., Morozova, I., Ignatieva, Y., and Cabaniss, J.: Russian anthropogenic black carbon:

Emission reconstruction and Arctic black carbon simulation, J. Geophys. Res. Atmos., 120, 11,306– 11,333, doi:10.1002/2015JD023358, 2015.

Hudson, P. K., Murphy, D. M., Cziczo, D. J., Thomson, D. S., de Gouw, J. A., Warneke, C., Holloway, J., Jost, H. J. and Hübler, G.: Biomass-burning particle measurements: Characteristics composition and chemical processing, J. Geophys. Res. D Atmos., 109(23), 1–11, doi:10.1029/2003JD004398, 2004.

Janssens-Maenhout, G., Crippa, M., Guizzardi, D., Dentener, F., Muntean, M., Pouliot, G., Keating, T., Zhang, Q., Kurokawa, J., Wankmüller, R., Denier van der Gon, H., Kuenen, J. J. P., Klimont, Z., Frost, G., Darras, S., Koffi, B., and Li, M.: HTAP_v2.2: a mosaic of regional and global emission grid maps for 2008 and 2010 to study hemispheric transport of air pollution, Atmos. Chem. Phys., 15, 11411–11432, https://doi.org/10.5194/acp-15-11411-2015, 2015.

Jimenez, J. L., Canagaratna, M. R., Donahue, N. M., Prevot, a. S. H., Zhang, Q., Kroll, J. H., DeCarlo, P. F., Allan, J. D., Coe, H., Ng, N. L., Aiken, a. C., Docherty, K. S., Ulbrich, I. M., Grieshop, A. P., Robinson, a. L., Duplissy, J., Smith, J. D., Wilson, K. R., Lanz, V. a., Hueglin, C., Sun, Y. L., Tian, J., Laaksonen, A., Raatikainen, T., Rautiainen, J., Vaattovaara, P., Ehn, M., Kulmala, M., Tomlinson, J. M., Collins, D. R., Cubison, M. J., Dunlea, E. J., Huffman, J. A., Onasch, T. B., Alfarra, M. R., Williams, P. I., Bower, K., Kondo, Y., Schneider, J., Drewnick, F., Borrmann, S., Weimer, S., Demerjian, K., Salcedo, D., Cottrell, L., Griffin, R., Takami, A., Miyoshi, T., Hatakeyama, S., Shimono, A., Sun, J. Y., Zhang, Y. M., Dzepina, K., Kimmel, J. R., Sueper, D., Jayne, J. T., Herndon, S. C., Trimborn, a. M., Williams, L. R., Wood, E. C., Middlebrook, A. M., Kolb, C. E., Baltensperger, U., Worsnop, D. R., Worsnop, D. R., Dunlea, J., Huffman, J. A., Onasch, T. B., Alfarra, M. R., Williams, P. I., Bower, K., Kondo, Y., Schneider, J., Drewnick, F., Borrmann, S., Weimer, S., Demerjian, K., Salcedo, D., Cottrell, L., Griffin, R., Takami, A., Miyoshi, T., Hatakeyama, S., Shimono, A., Sun, J. Y., Zhang, Y. M., Dzepina, K., Kimmel, J. R., Sueper, D., Jayne, J. T., Herndon, S. C., Trimborn, a. M., Williams, L. R., Wood, E. C., Middlebrook, A. M., Kolb, C. E., Baltensperger, U., Worsnop, D. R., Dunlea, E. J., et al.: Evolution of Organic Aerosols in the Atmosphere, Science 80., 326(5959), 1525–1529, doi:10.1126/science.1180353, 2009.

Jolleys, M. D., Coe, H., McFiggans, G., Taylor, J. W., O'Shea, S. J., Le Breton, M., Bauguitte, S. J.-B., Moller, S., Di Carlo, P., Aruffo, E., Palmer, P. I., Lee, J. D., Percival, C. J. and Gallagher, M. W.: Properties and evolution of biomass burning organic aerosol

from Canadian boreal forest fires, Atmos. Chem. Phys., 15(6), 3077–3095, doi:10.5194/acp-15-3077-2015, 2015.

Kaiser, J. W., Heil, A., Andreae, M. O., Benedetti, A., Chubarova, N., Jones, L., Morcrette, J.-J., Razinger, M., Schultz, M. G., Suttie, M., and van der Werf, G. R.: Biomass burning emissions estimated with a global fire assimilation system based on observed fire radiative power, Biogeosciences, 9, 527–554, https://doi.org/10.5194/bg-9-527-2012, https://www.biogeosciences.net/9/527/2012/, 2012.

Kanakidou, M., Seinfeld, J. H., Pandis, S. N., Barnes, I., Dentener, F. J., Facchini, M. C., Van Dingenen, R., Ervens, B., Nenes, A., Nielsen, C. J., Swietlicki, E., Putaud, J. P., Balkanski, Y., Fuzzi, S., Horth, J., Moortgat, G. K., Winterhalter, R., Myhre, C. E. L., Tsigaridis, K., Vignati, E., Stephanou, E. G., and Wilson, J.: Organic aerosol and global climate modelling: a review, Atmos. Chem. Phys., 5, 1053-1123, https://doi.org/10.5194/acp-5-1053-2005, 2005.

Katich, J. M., Samset, B. H., Paul Bui, T., Dollner, M., Froyd, K.D., Campuzano-Jost, P., Nault, B. A., Schroder, J. C., Weinzierl, B., Schwarz, J. P.: Strong Contrast in Remote Black Carbon Aerosol Loadings Between the Atlantic and Pacific Basins, J. Geophys. Res. Atmos., 123 (23), pages 13,386-13,395, https://doi.org/10.1029/2018JD029206, 2018.

Kim, M. J., G. A. Novak, M. C. Zoerb,M. Yang, B. W. Blomquist, B. J. Huebert, C. D. Cappa, and T. H. Bertram: Air-Sea exchange of biogenic volatile organic compounds and the impact on aerosol particle size distributions, Geophys. Res. Lett.,44, 3887–3896, doi:10.1002/2017GL072975, 2017.

Klimont, Z., K. Kupiainen, C. Heyes, P. Purohit, J. Cofala, P. Rafaj, J. Borken-Kleefeld, and W. Schöpp,: Global anthropogenic emissions of particulate matter including black carbon, Atmos. Chem. Phys., 17(14), 8681-8723, doi: 10.5194/acp-17-8681-2017, 2017.

Kodros, J. K., Cucinotta, R., Ridley, D. A., Wiedinmyer, C., and Pierce, J. R.: The aerosol radiative effects of uncontrolled combustion of domestic waste, Atmos. Chem. Phys., 16, 6771-6784, https://doi.org/10.5194/acp-16-6771-2016, 2016.

Krechmer, J.E., D. Pagonis, P.J. Ziemann, and J.L. Jimenez. Quantification of gas-wall partitioning in Teflon environmental chambers using rapid bursts of low-volatility oxidized species generated in-situ. Environmental Science and Technology, 50, 5757–5765, doi:10.1021/acs.est.6b00606, 2016.

Kroll, J. H., Donahue, N. M., Jimenez, J. L., Kessler, S. H., Canagaratna, M. R., Wilson, K. R., Altieri, K. E., Mazzoleni, L. R., Wozniak, A. S., Bluhm, H., Mysak, E. R., Smith, J. D., Kolb, C. E. and Worsnop, D. R.: Carbon oxidation state as a metric for describing the chemistry of atmospheric organic aerosol., Nat. Chem., 3(2), 133–9, doi:10.1038/nchem.948, 2011.

Laskin, A., Laskin, J., and Nizkorodov, S.: Chemistry of Atmospheric Brown Carbon, Chem. Rev. 2015, 115, 10, 4335-4382, 2015.

Lee, A. K. Y., Willis, M. D., Healy, R. M., Onasch, T. B., and Abbatt, J. P. D.: Mixing state of carbonaceous aerosol in an urban environment: single particle characterization using the soot particle aerosol mass spectrometer (SP-AMS), Atmos. Chem. Phys., 15, 1823-1841, https://doi.org/10.5194/acp-15-1823-2015, 2015.

Liu, H. Y., D. J. Jacob, I. Bey, and R. M. Yantosca: Constraints from Pb-210 and Be-7 on wet deposition and transport in a global three-dimensional chemical tracer model driven by assimilated meteorological fields, J. Geophys. Res., 106(D11), 12,109–12,128, 2001.

Liu, X., Easter, R. C., Ghan, S. J., Zaveri, R., Rasch, P., Shi, X., Lamarque, J.-F., Gettelman, A., Morrison, H., Vitt, F., Conley, A., Park, S., Neale, R., Hannay, C., Ekman, A. M. L., Hess, P., Mahowald, N., Collins, W., Iacono, M. J., Bretherton, C. S., Flanner, M. G., and Mitchell, D.: Toward a minimal representation of aerosols in climate models: description and evaluation in the Community Atmosphere Model CAM5, Geosci. Model Dev., 5, 709-739, https://doi.org/10.5194/gmd-5-709-2012, 2012.

Marais, E. A., Jacob, D. J., Jimenez, J. L., Campuzano-Jost, P., Day, D. A., Hu, W., Krechmer, J., Zhu, L., Kim, P. S., Miller, C. C., Fisher, J. A., Travis, K., Yu, K., Hanisco, T. F., Wolfe, G. M., Arkinson, H. L., Pye, H. O. T., Froyd, K. D., Liao, J., and McNeill, V. F.: Aqueous-phase mechanism for secondary organic aerosol formation from isoprene: application to the southeast United States and co-benefit of SO2 emission controls, Atmos. Chem. Phys., 16, 1603-1618, https://doi.org/10.5194/acp-16-1603-2016, 2016.

Myhre, G., Samset, B. H., Schulz, M., Balkanski, Y., Bauer, S., Berntsen, T. K., Bian, H., Bellouin, N., Chin, M., Diehl, T., Easter, R. C., Feichter, J., Ghan, S. J., Hauglustaine, D., Iversen, T., Kinne, S., Kirkevåg, A., Lamarque, J.-F., Lin, G., Liu, X., Lund, M. T., Luo, G., Ma, X., van Noije, T., Penner, J. E., Rasch, P. J., Ruiz, A., Seland, Ø., Skeie, R. B., Stier, P., Takemura, T., Tsigaridis, K., Wang, P., Wang, Z., Xu, L., Yu, H., Yu, F., Yoon, J.-H., Zhang, K., Zhang, H., and Zhou, C.: Radiative forcing of the direct aerosol effect from

AeroCom Phase II simulations, Atmos. Chem. Phys., 13, 1853-1877, https://doi.org/10.5194/acp-13-1853-2013, 2013.

Mauderly, J. L., & Chow, J. C: Health Effects of Organic Aerosols, Inhalation Toxicology, 20:3, 257-288, DOI: 10.1080/08958370701866008, 2008.

Middlebrook, A. M., Murphy, D. M. and Thomson, D. S.: Observations of organic material in individual marine particles at Cape Grim during the First Aerosol Characterization Experiment (ACE 1), J. Geophys. Res. Atmos., 103(D13), 16475–16483, doi:10.1029/97JD03719, 1998.

Murphy, D. M., Froyd, K. D., Bian, H., Brock, C. A., Dibb, J. E., DiGangi, J. P., Diskin, G., Dollner, M., Kupc, A., Scheuer, E. M., Schill, G. P., Weinzierl, B., Williamson, C. J., and Yu, P.: The distribution of sea-salt aerosol in the global troposphere, Atmos. Chem. Phys., 19, 4093-4104, https://doi.org/10.5194/acp-19-4093-2019, 2019.

Nault, B. A., Campuzano-Jost, P., Day, D. A., Schroder, J. C., Anderson, B., Beyersdorf, A. J., Blake, D. R., Brune, W. H., Choi, Y., Corr, C. A., de Gouw, J. A., Dibb, J., DiGangi, J. P., Diskin, G. S., Fried, A., Huey, L. G., Kim, M. J., Knote, C. J., Lamb, K. D., Lee, T., Park, T., Pusede, S. E., Scheuer, E., Thornhill, K. L., Woo, J.-H., and Jimenez, J. L.: Secondary organic aerosol production from local emissions dominates the organic aerosol budget over Seoul, South Korea, during KORUS-AQ, Atmos. Chem. Phys., 18, 17769-17800, https://doi.org/10.5194/acp-18-17769-2018, 2018.

Ovadnevaite, J., Ceburnis, D., Canagaratna, M., Berresheim, H., Bialek, J., Martucci, G., Worsnop, D. R. and O'Dowd, C.: On the effect of wind speed on submicron sea salt mass concentrations and source fluxes, J. Geophys. Res. Atmos., 117(D16), 1–11, doi:10.1029/2011JD017379, 2012.

Petters, M. D., Prenni, A. J., Kreidenweis, S. M., DeMott, P. J., Matsunaga, A., Lim, Y. B., and Ziemann, P. J. Chemical aging and the hydrophobic-to-hydrophilic conversion of carbonaceous aerosol, Geophys. Res. Lett., 33, L24806, doi:10.1029/2006GL027249, 2006.

Palm, B. B., de Sá, S. S., Day, D. A., Campuzano-Jost, P., Hu, W., Seco, R., Sjostedt, S. J., Park, J.-H., Guenther, A. B., Kim, S., Brito, J., Wurm, F., Artaxo, P., Thalman, R., Wang, J., Yee, L. D., Wernis, R., Isaacman-VanWertz, G., Goldstein, A. H., Liu, Y., Springston, S. R., Souza, R., Newburn, M. K., Alexander, M. L., Martin, S. T., and Jimenez, J. L.: Secondary organic aerosol formation from ambient air in an oxidation flow reactor in

central Amazonia, Atmos. Chem. Phys., 18, 467–493, https://doi.org/10.5194/acp-18-467-2018, 2018.

Pye, H. O. T., Chan, A. W. H., Barkley, M. P., and Seinfeld, J. H.: Global modeling of organic aerosol: The importance of reactive nitrogen (NOx and NO_3), Atmos. Chem. Phys., 10, 11,261–11,276, doi:10.5194/acp-10-11261-2010, 2010.

Robinson, A. L., Donahue, N. M., Shrivastava, M. K., Weitkamp, E. A., Sage, A. M., Grieshop, A. P., Lane, T. E., Pandis, S. N., and Pierce, J. R.: Rethinking organic aerosols: Semivolatile emissions and photochemical aging, Science, 315, 1259–1262, 2007.

Schroder, J. C., Campuzano-Jost, P., Day, D. A., Shah, V., Larson, K., Sommers, J. M., Sullivan, A. P., Campos, T., Reeves, J. M., Hills, A., Hornbrook, R. S., Blake, N. J., Scheuer, E., Guo, H., Fibiger, D. L., McDuffie, E. E., Hayes, P. L., Weber, R. J., Dibb, J. E., Apel, E. C., Jaeglé, L., Brown, S. S., Thornton, J. A. and Jimenez, J. L.: Sources and Secondary Production of Organic Aerosols in the Northeastern United States during WINTER, J. Geophys. Res. Atmos., 123(14), 7771–7796, doi:10.1029/2018JD028475, 2018.

Schacht, J., Heinold, B., Quaas, J., Backman, J., Cherian, R., Ehrlich, A., Herber, A., Huang, W. T. K., Kondo, Y. Massling, A, Sinha, P.R., Weinzierl, B. Zanatta, M., and Tegen, I.: The importance of the representation of air pollution emissions for the modeled distribution and radiative effects of black carbon in the Arctic, Atmos. Chem. Phys. Discuss., 2019, 1-39, doi: 10.5194/acp-2019-71, 2019.

Schulz, M., Chin, M., and Kinne, S.: The aerosol model comparison project, AeroCom, phase II: clearing up diversity, IGAC newsletter, No. 41, 2–11, 2009.

Scott, C. E., Rap, A., Spracklen, D. V., Forster, P. M., Carslaw, K. S., Mann, G. W., Pringle, K. J., Kivekäs, N., Kulmala, M., Lihavainen, H., and Tunved, P.: The direct and indirect radiative effects of biogenic secondary organic aerosol, Atmos. Chem. Phys., 14, 447-470, https://doi.org/10.5194/acp-14-447-2014, 2014.

Shah, V., Jaeglé, L., Jimenez, J. L., Schroder, J. C., Campuzano-Jost, P., Campos, T. L., et al.: Widespread pollution from secondary sources of organic aerosols during winter in the Northeastern United States. Geophysical Research Letters, 46, 2974– 2983. https://doi.org/10.1029/2018GL081530, 2019.

Shiraiwa, M., Ueda, K., Pozzer, A., Lammel, G., Kampf, C. J.: Aerosol Health Effects from Molecular to Global Scales, Environ. Sci. Technol. 51 (23), pp 13545–13567, 2017.

Shrivastava, M., Cappa, C.D., Fan, J., et al: Recent advances in understanding secondary organic aerosol: Implications for global climate forcing, Rev. Geophys., 55, 509–559, doi:10.1002/2016RG000540, 2017.

Spracklen, D. V., Jimenez, J. L., Carslaw, K. S., Worsnop, D. R., Evans, M. J., Mann, G. W., Zhang, Q., Canagaratna, M. R., Allan, J., Coe, H., McFiggans, G., Rap, A., and Forster, P.: Aerosol mass spectrometer constraint on the global secondary organic aerosol budget, Atmos. Chem. Phys., 11, 12109–12136, doi:10.5194/acp-11-12109-2011, 2011.

Tegen, I., Neubauer, D., Ferrachat, S., Siegenthaler-Le Drian, C., Bey, I., Schutgens, N., Stier, P., Watson-Parris, D., Stanelle, T., Schmidt, H., Rast, S., Kokkola, H., Schultz, M., Schroeder, S., Daskalakis, N., Barthel, S., Heinold, B., and Lohmann, U.: The global aerosol–climate model ECHAM6.3–HAM2.3 – Part 1: Aerosol evaluation, Geosci. Model Dev., 12, 1643-1677, https://doi.org/10.5194/gmd-12-1643-2019, 2019.

Thomson, D. S., Schein, M. E. and Murphy, D. M.: Particle Analysis by Laser Mass Spectrometry WB-57F Instrument Overview, Aerosol Sci. Technol., 33(1–2), 153–169, doi:10.1080/027868200410903, 2000.

Tilmes, S., Hodzic, A., Emmons, L.K., Mills, M.J., Gettelman, A., Kinnison, D.E., Park, M., Lamarque J.-F., Vitt, F., et al.: Climate forcing and trends of organic aerosols in the Community Earth System Model (CESM2), to be submitted to JAMES, 2019.

Tsigaridis, K., Daskalakis, N., Kanakidou, M., Adams, P. J., Artaxo, P., Bahadur, R., Balkanski, Y., Bauer, S. E., Bellouin, N., Benedetti, A., Bergman, T., Berntsen, T. K., Beukes, J. P., Bian, H., Carslaw, K. S., Chin, M., Curci, G., Diehl, T., Easter, R. C., Ghan, S. J., Gong, S. L., Hodzic, A., Hoyle, C. R., Iversen, T., Jathar, S., Jimenez, J. L., Kaiser, J. W., Kirkevåg, A., Koch, D., Kokkola, H., Lee, Y. H., Lin, G., Liu, X., Luo, G., Ma, X., Mann, G. W., Mihalopoulos, N., Morcrette, J.-J., Müller, J.-F., Myhre, G., Myriokefalitakis, S., Ng, N. L., O'Donnell, D., Penner, J. E., Pozzoli, L., Pringle, K. J., Russell, L. M., Schulz, M., Sciare, J., Seland, Ø., Shindell, D. T., Sillman, S., Skeie, R. B., Spracklen, D., Stavrakou, T., Steenrod, S. D., Takemura, T., Tiitta, P., Tilmes, S., Tost, H., van Noije, T., van Zyl, P. G., von Salzen, K., Yu, F., Wang, Z., Wang, Z., Zaveri, R. A., Zhang, H., Zhang, K., Zhang, Q., and Zhang, X.: The AeroCom evaluation and intercomparison of organic

aerosol in global models, Atmos. Chem. Phys., 14, 10845–10895, doi:10.5194/acp-14-10845-2014, 2014.

Tsigaridis, K., and Kanakidou, M.: The Present and Future of Secondary Organic Aerosol Direct Forcing on Climate, Current Climate Change Reports, 2018, Volume 4, Issue 2, pp 84–98, 2018.

Turpin, B. J. and Lim, H. J.: Species contributions to PM2.5 mass concentrations: Revisiting common assumptions for estimating organic mass, Aerosol Sci. Tech., 35, 602–610, doi:10.1080/02786820152051454, 2001.

Ulbrich, I. M., Canagaratna, M. R., Zhang, Q., Worsnop, D. R. and Jimenez, J. L.: Interpretation of organic components from Positive Matrix Factorization of aerosol mass spectrometric data, Atmos. Chem. Phys., 9(9), 2891–2918, doi:10.5194/acp-9-2891-2009, 2009.

van der Werf, G. R., Randerson, J. T., Giglio, L., Collatz, G. J., Mu, M., Kasibhatla, P. S., Morton, D. C., DeFries, R. S., Jin, Y., and van Leeuwen, T. T.: Global fire emissions and the contribution of deforestation, savanna, forest, agricultural, and peat fires (1997–2009), Atmos. Chem. Phys., 10, 11707-11735, https://doi.org/10.5194/acp-10-11707-2010, 2010.

Vergara-Temprado, J., Murray, B. J., Wilson, T. W., O'Sullivan, D., Browse, J., Pringle, K. J., Ardon-Dryer, K., Bertram, A. K., Burrows, S. M., Ceburnis, D., DeMott, P. J., Mason, R. H., O'Dowd, C. D., Rinaldi, M., and Carslaw, K. S.: Contribution of feldspar and marine organic aerosols to global ice nucleating particle concentrations, Atmos. Chem. Phys., 17, 3637-3658, https://doi.org/10.5194/acp-17-3637-2017, 2017.

Wang, J., Cubison, M. J., Aiken, A. C., Jimenez, J. L., and Collins, D. R.: The importance of aerosol mixing state and size-resolved composition on CCN concentration and the variation of the importance with atmospheric aging of aerosols, Atmos. Chem. Phys., 10, 7267-7283, https://doi.org/10.5194/acp-10-7267-2010, 2010.

Williamson, C. J., Kupc, A., Axisa, D., Bilsback, K.R., Bui, T., Campuzano-Jost, P., Dollner, M., Froyd, K., Hodshire, A. L., Jimenez, J. L., Kodros, J. K., Luo, G., Murphy, D. M., Nault, B. A., Ray, E. A., Weinzierl, B. B., Wilson, J. C., Yu, F., Yu, P., Pierce, J.F., Brock C. A.: A Large Source of Cloud Condensation Nuclei from New Particle Formation in the Tropics, submitted to Nature, 2019.

Wofsy, S.C., S. Afshar, H.M. Allen, E. Apel, E.C. Asher, B. Barletta, J. Bent, H. Bian, B.C. Biggs, D.R. Blake, N. Blake, I. Bourgeois, C.A. Brock, W.H. Brune, J.W. Budney, T.P. Bui, A. Butler, P. Campuzano-Jost, C.S. Chang, M. Chin, R. Commane, G. Correa, J.D. Crounse, P. D. Cullis, B.C. Daube, D.A. Day, J.M. Dean-Day, J.E. Dibb, J.P. DiGangi, G.S. Diskin, M. Dollner, J.W. Elkins, F. Erdesz, A.M. Fiore, C.M. Flynn, K. Froyd, D.W. Gesler, S.R. Hall, T.F. Hanisco, R.A. Hannun, A.J. Hills, E.J. Hintsa, A. Hoffman, R.S. Hornbrook, L.G. Huey, S. Hughes, J.L. Jimenez, B.J. Johnson, J.M. Katich, R.F. Keeling, M.J. Kim, A. Kupc, L.R. Lait, J.-F. Lamarque, J. Liu, K. McKain, R.J. Mclaughlin, S. Meinardi, D.O. Miller, S.A. Montzka, F.L. Moore, E.J. Morgan, D.M. Murphy, L.T. Murray, B.A. Nault, J.A. Neuman, P.A. Newman, J.M. Nicely, X. Pan, W. Paplawsky, J. Peischl, M.J. Prather, D.J. Price, E. Ray, J.M. Reeves, M. Richardson, A.W. Rollins, K.H. Rosenlof, T.B. Ryerson, E. Scheuer, G.P. Schill, J.C. Schroder, J.P. Schwarz, J.M. St.Clair, S.D. Steenrod, B.B. Stephens, S.A. Strode, C. Sweeney, D. Tanner, A.P. Teng, A.B. Thames, C.R. Thompson, K. Ullmann, P.R. Veres, N. Vieznor, N.L. Wagner, A. Watt, R. Weber, B. Weinzierl, P. Wennberg, C.J. Williamson, J.C. Wilson, G.M. Wolfe, C.T. Woods, and L.H. Zeng. 2018. ATom: Merged Atmospheric Chemistry, Trace Gases, and Aerosols. ORNL DAAC, Oak Ridge, Tennessee, USA. https://doi.org/10.3334/ORNLDAAC/1581, 2018.

Woody, M. C., Baker, K. R., Hayes, P. L., Jimenez, J. L., Koo, B., and Pye, H. O. T.: Understanding sources of organic aerosol during CalNex-2010 using the CMAQ-VBS, Atmos. Chem. Phys., 16, 4081-4100, https://doi.org/10.5194/acp-16-4081-2016, 2016.

Yu, P., O. B. Toon, C. G. Bardeen, M. J. Mills, T. Fan, J. M. English, and R. R. Neely, Evaluations of tropospheric aerosol properties simulated by the community earth system model with a sectional aerosol microphysics scheme, J. Adv. Model. Earth Syst.,7, 865–914, doi:10.1002/2014MS000421, 2015.

Yu, P., Froyd, K. D., Portmann, R. W., Toon, O. B., Freitas, S. R., Bardeen, C. G., et al.: Efficient in-cloud removal of aerosols by deep convection. Geophysical Research Letters, 46. https://doi.org/10.1029/2018GL080544, 2019.

Zhang, K., O'Donnell, D., Kazil, J., Stier, P., Kinne, S., Lohmann, U., Ferrachat, S., Croft, B., Quaas, J., Wan, H., Rast, S., and Feichter, J.: The global aerosol-climate model ECHAM-HAM, version 2: sensitivity to improvements in process representations, Atmos. Chem. Phys., 12, 8911-8949, https://doi.org/10.5194/acp-12-8911-2012, 2012.

https://doi.org/10.5194/acp-2019-773
Preprint. Discussion started: 20 September 2019

Zhang, Q. J., Beekmann, M., Drewnick, F., Freutel, F., Schneider, J., Crippa, M., Prevot, A. S. H., Baltensperger, U., Poulain, L., Wiedensohler, A., Sciare, J., Gros, V., Borbon, A., Colomb, A., Michoud, V., Doussin, J.-F., Denier van der Gon, H. A. C., Haeffelin, M., Dupont, J.-C., Siour, G., Petetin, H., Bessagnet, B., Pandis, S. N., Hodzic, A., Sanchez, O., Honoré, C., and Perrussel, O., 2013. Formation of organic aerosol in the Paris region during the MEGAPOLI summer campaign: evaluation of the volatility-basis-set approach within the CHIMERE model, Atmos. Chem. Phys., 13, 5767-5790, doi:10.5194/acp-13-5767-2013.

Zhang, X., Cappa, C. D., Jathar, S. H., McVay, R. C., Ensberg, J. J., Kleeman, M. J., and Seinfeld, J. H.: Influence of vapor wall loss in laboratory chambers on yields of secondary organic aerosol, P. Natl. Acad. Sci. USA, 111, 5802–5807, 2014.

Zotter, P., I. El-Haddad, Y. Zhang, P.L. Hayes, X. Zhang, Y.H. Lin, L. Wacker, J. Schnelle-Kreis, G. Abbaszade, R. Zimmermann, J.D. Surratt, R. Weber, J.L. Jimenez, S. Szidat, U. Baltensperger, A.S.H. Prévôt. Diurnal cycle of fossil and non-fossil carbon using radiocarbon analyses during CalNex. Journal of Geophysical Research-Atmospheres, 119, 6818–6835, doi:10.1002/2013JD021114, 2014.

https://doi.org/10.5194/acp-2019-773
Preprint. Discussion started: 20 September 2019

Atmospheric Chemistry and Physics Discussions

Tables

Table 1: ATom global model configurations and their treatment of the most important processes affecting organic aerosols.

Models & horizontal res. & config. reference	Aerosol module	Submicron size[6] OA (dust/seasalt)	SOA precursors[1]					SOA production	Emission	Removal		
			ISO	MT	SQ	ANT	$C_{>12}$			Standard[2]	Improved	Photolytic
CESM1-CARMA (1.9° lon x 2.5° lat) (Yu et al. 2019)	20 bins	< 500 nm (< 800 nm)	x	x		x		Semi-volatile using VBS (Pye et al. 2010)	GAIS and GFED v3	x	For convective updrafts (Yu et al. 2019)[3]	
CESM2-DYN (0.9° lon x 1.25° lat) (Tilmes et al. 2019)	4 modes	< 270 nm (< 800 nm)	x	x	x	x	x	Semi-volatile using VBS (Hodzic et al. 2016)	CMIP6 and QFED v2.4	x	Water solubility of organic gases per Hodzic et al. (2014)	For SOA (Hodzic et al. 2016)
CESM2-SMP (0.9° lon x 1.25° lat) (Tilmes et al. 2019)	4 modes	< 270 nm (< 800 nm)	x	x		x		Non-volatile with prescribed mass yields for all precursors[4]	CMIP6 and QFED v2.4	x		
ECHAM6-HAM (1.87°lon x1.87°lat) (Tegen et al. 2019)	7 modes	< 500 nm (< 500 nm)		x				Non-volatile with 15% prescribed mass yields (Dentener et al. 2006)	ECLIPSE[5] and GFAS	x		
GC12-REF (2° lon x 2.5° lat) (Bey et al. 2001)	Bulk	Bulk (< 500 nm)	x	x	x	x		Semi-volatile using VBS (Pye et al. 2010); non-volatile isoprene-SOA	CMIP6 and GFED v4	x	For convective updrafts per Wang et al. 2014	

https://doi.org/10.5194/acp-2019-773
Preprint. Discussion started: 20 September 2019

								(Marais et al. 2016)				
GC12-DYN (2° lon x 2.5° lat) (Bey et al. 2001)	Bulk	Bulk (< 500 nm)	x	x	x	x	x	Semi-volatile using VBS (Hodzic et al. 2016); non-volatile isoprene-SOA (Marais et al. 2016)	CMIP6 and GFED v4	x	For convective updrafts (Wang et al. 2014); Water solubility of organic gases (Hodzic et al. 2014)	For SOA (Hodzic et al. 2016)
GC10-TOMAS (5° lon x 4° lat) (Kodros et al. 2016)	15 bins	< 316 nm (< 316 nm)		x		x		Non-Volatile using 10% mass yields for MT, 0.2 Tg SOA per Tg CO for anthropogenic emissions	EDGAR v4 and GFED v3	x	For convective updrafts (Wang et al. 2014)	
GEOS5-GOCART (0.5° lon x 0.625°lat) (Bian et al. 2019)	Bulk	bulk (< 730 nm for dust, 316 nm for seasalt)	x	x		x		Non-Volatile, 10% mass yields for all precursors	HTAP and QFED v2.54	x		

(1) SOA precursors include isoprene (ISO), monoterpenes (MT), sesquiterpenes (SQ), anthropogenics (ANT) including aromatics such as benzene, toluene and xylene, as well as lumped shorter chain alkanes and alkenes; and higher molecular weight n-alkanes and n-alkenes (C>12).
(2) Standard removal includes dry deposition and sedimentation, as well as convective and large-scale scavenging of soluble organic gases and aerosols, and below-cloud scavenging of aerosols.
(3) A sensitivity simulation is performed with CESM1-CARMA without the improved scavenging in convective updrafts.
(4) 5% for lumped C<12 alkanes, 5% for lumped C<12 alkenes, 15% for aromatics, 4% for isoprene, 25% for monoterpenes.
(5) Anthropogenic BC emission are replaced in Russia with the dataset of Huang et al. (2015).
(6) Submicron size range (diameter) used in various models for comparison with the AMS data.

https://doi.org/10.5194/acp-2019-773
Preprint. Discussion started: 20 September 2019

Table 2: Comparison of observed and simulated OA concentrations along ATom-1 and ATom-2 flights for eight global model simulations and their ensemble. The results of the model ensemble are also indicated. The statistical indicators are calculated as normalized mean bias $NMB(\%) = 100 \times \sum_i (M_i - O_i) / \sum_i O_i$; normalized mean error $NME(\%) = 100 \times \sum_i |(M_i - O_i)| / \sum_i O_i$; root mean square error $RMSE(\mu g\, m^{-3}) = \sqrt{(1/N) \sum_i (M_i - O_i)^2}$ and correlation coefficient (R^2) between modeled (M_i) and observed (O_i) data points. The mean of ATom-1 observations is ~0.23 μg m^{-3} and for ATom-2 is 0.11 μg m^{-3}. Figure S4 shows the normalized mean bias for all individual ATom model simulations for various latitudinal regions and for both the Atlantic and Pacific basins.

Organic aerosols	Avg.Mod. (μg m^{-3})	NMB (%)	NME (%)	RMSE (μg m^{-3})	R^2	Avg.Mod. (μg m^{-3})	NMB (%)	NME (%)	RMSE (μg m^{-3})	R^2
Model	*ATom-1 scores (August 2016)*					*ATom-2 scores (February 2017)*				
AeroCom-II Ens.	0.400	74.2	127.3	0.560	0.31	0.254	137	175	0.278	0.38
AeroCom-II Sub.(1)	0.335	47.0	111	0.557	0.28	0.242	127	178	0.290	0.27
ATom Ensemble	0.239	-4.5	64.6	0.372	0.66	0.139	23	92.6	0.224	0.48
CESM2-DYN	0.268	4.6	83.7	0.867	0.47	0.140	25.6	111.7	0.317	0.36
CESM2-SMP	0.349	36.3	94.3	0.556	0.51	0.175	57.2	125.4	0.299	0.31
CESM1-CARMA	0.155	-33.2	93.8	0.603	0.12	0.131	22.6	119.6	0.244	0.31
ECHAM6-HAM	0.400	73.6	143.6	0.714	0.24	0.214	100	184.0	0.363	0.23
GC12-DYN	0.142	-32.6	79.4	0.560	0.16	0.174	14.7	96.6	0.312	0.39
GC12-REF	0.122	-43.0	76.5	0.536	0.18	0.147	3.6	96.3	0.292	0.35
GC10-TOMAS	0.218	-14.4	86.5	0.644	0.16	0.313	150.0	223.7	0.537	0.12
GEOS5-GOCART	0.242	-5.4	86.6	0.975	0.38	0.084	-24.9	86.4	0.268	0.29

(1) This is the subset of AeroCom-II model ensemble that includes only seven models that are similar to those that are included in the ATom ensemble (either the same model, or an older model version, or the same aerosol module). AeroCom-II Sub. incudes CAM5-MAM3, CCSM4-hem, ECHAM5-HAM2,

https://doi.org/10.5194/acp-2019-773
Preprint. Discussion started: 20 September 2019

GEOSChem-APM 8.2, GEOSChem 9, GISS-TOMAS and GMI (see Tsigaridis et al., 2014 for their description).

https://doi.org/10.5194/acp-2019-773
Preprint. Discussion started: 20 September 2019

Figures:

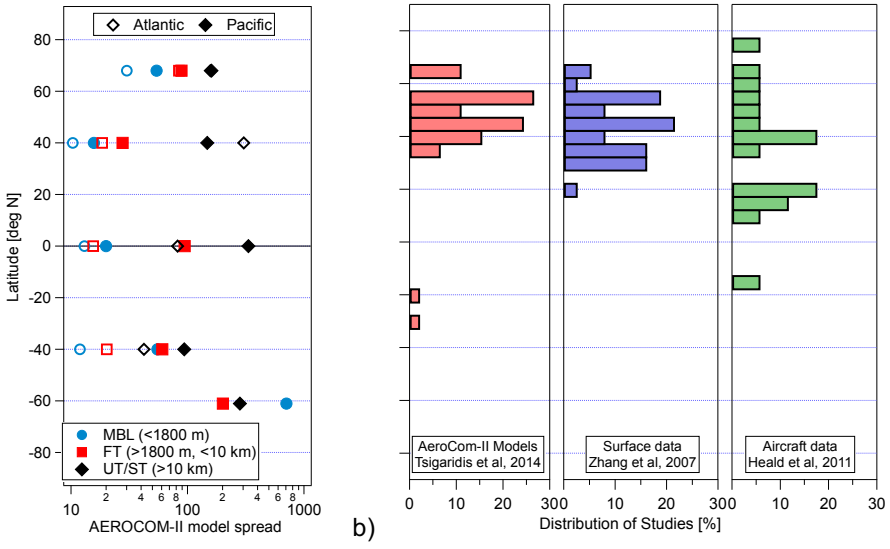

a) b)

Figure 1: (a, left) The ratio between the highest and the lowest OA concentrations as predicted among 28 global chemistry transport models participating in the AeroCom phase II intercomparison study (Tsigaridis et al. 2014); (b, right) Percent distribution of AeroCom-II models (author affiliations) and of measurements from two literature overview studies (Zhang et al., 2007; Heald et al., 2011) for the OA ground and aircraft AMS as a function of latitude. For the aircraft campaigns, the average latitude for the full deployment was taken.

https://doi.org/10.5194/acp-2019-773
Preprint. Discussion started: 20 September 2019

Atmospheric Chemistry and Physics Discussions
Open Access
EGU

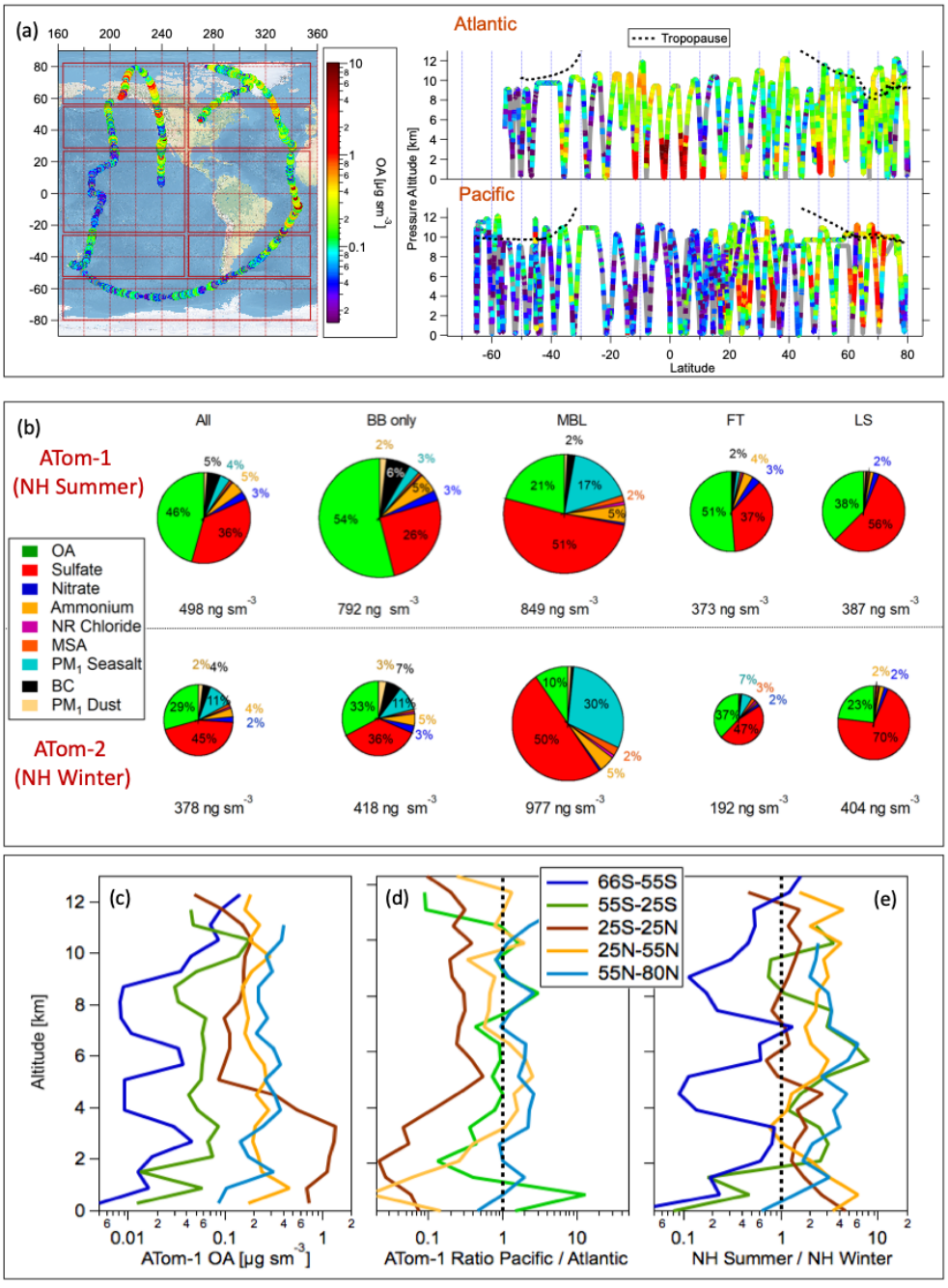

1414

https://doi.org/10.5194/acp-2019-773
Preprint. Discussion started: 20 September 2019

Figure 2: (a, left) ATom-1 DC-8 flights during the August 2016 deployment. Red boxes indicate regions used for the latitude averaging of the model results. (a, right) Vertical distribution of OA concentrations (μg sm^{-3}) along ATom-1 flight tracks (b) Average submicron aerosol composition as measured in the biomass-burning influenced regions (BB only), and the non-BB influenced regions including the marine boundary layer (MBL), free troposphere (FT), and lower stratosphere (LS) for ATom-1 (upper plots) and ATom-2 (lower plots). The BB influenced airmasses were filtered using the PALMS data (see section 3.1). Contributions below 2% are shown but not labeled on the pie chart graph. (c) The average OA vertical profiles are shown for each latitude region as well as (d) the ratios between the Pacific and Atlantic Oceans in each region. (e) The seasonal contrast in OA concentrations as calculated as the ratio in OA concentrations between the NH summer (ATom-1) and NH winter (ATom-2) campaigns. The corresponding plots for ATom-2 can be found in Fig. S1.

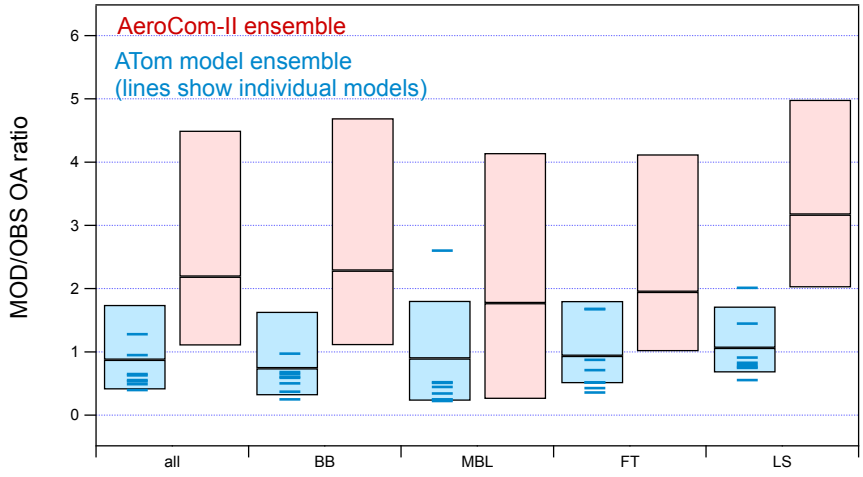

Figure 3: Ratios between predicted and observed OA concentrations for all ATom-1 flights as calculated for the ATom and AeroCom-II model ensembles in different regions ("BB" biomass burning influenced regions; "MBL" clean marine boundary layer; "FT" clean free troposphere' and "LS" lower stratosphere). Median of the ensemble ratio is shown as a horizontal line, while the boxes indicate 25th and 75th percentiles. Medians for the individual models included in the current ATom model ensemble are also shown as blue lines.

https://doi.org/10.5194/acp-2019-773
Preprint. Discussion started: 20 September 2019

Atmospheric Chemistry and Physics Discussions
Open Access
EGU

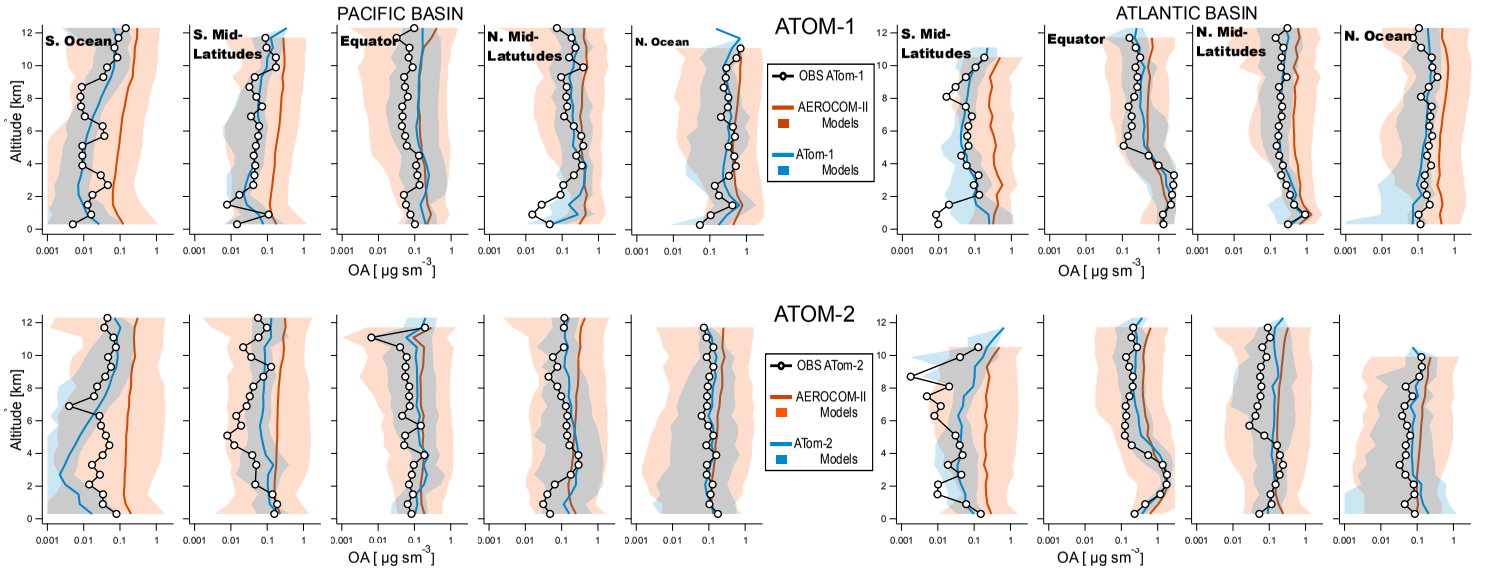

Figure 4: Comparison of latitude-averaged predicted OA vertical profiles with ATom-1 and -2 measurements taken over the Pacific (left side) and Atlantic (right side) basins. Results of the AeroCom-II model ensemble average are shown in red while those of the ATom model ensemble are shown in blue. Shaded areas indicate the variability (two standard deviations) within each model ensemble.

https://doi.org/10.5194/acp-2019-773
Preprint. Discussion started: 20 September 2019

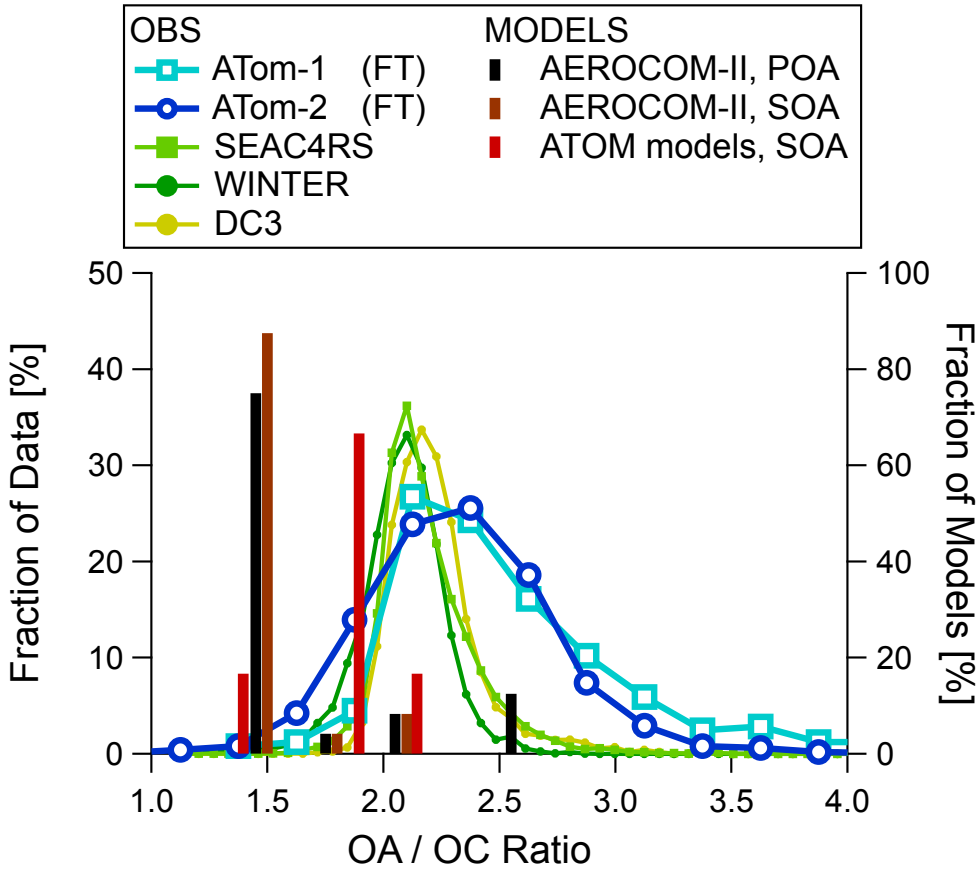

Figure 5: Distribution of the OA / OC ratio as measured during ATom-1 and -2. Values for the recent aircraft campaigns (SEAC4RS, DC3 and WINTER) that took place over continental US regions closer to continental source regions are also shown (Schroder et al., 2018). The bars (right axis) show the OA/OC used for SOA and POA by the models included in the AeroCom and ATom ensemble, with OA/OC=1.4 being the modal value for the former and 1.8 for the latter.

https://doi.org/10.5194/acp-2019-773
Preprint. Discussion started: 20 September 2019

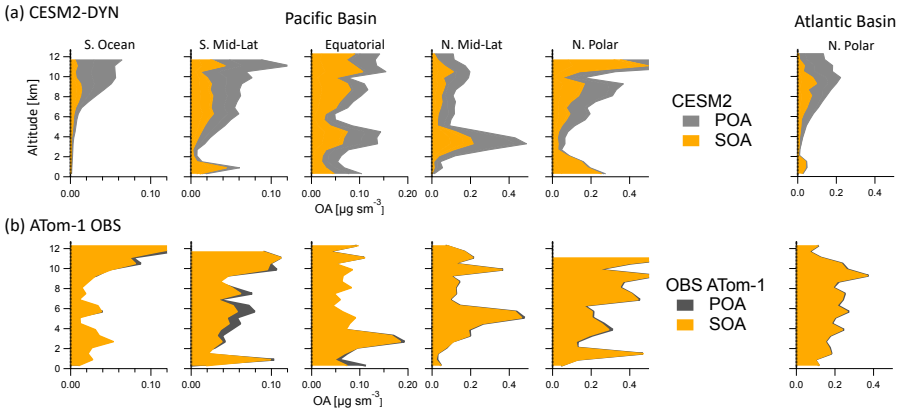

Figure 6: Comparison of averaged POA and SOA vertical profiles as observed during ATom and as predicted by the CESM2-DYN model over the non-BB influenced Pacific and Atlantic basins. The comparison is not shown for the strongly biomass burning influenced regions as all the OA is conservatively allocated to POA in those regions.

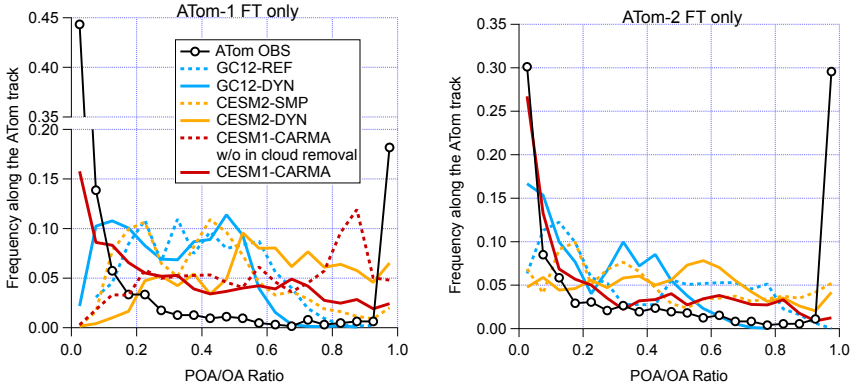

Figure 7: Frequency distribution of observed and simulated ratio of POA to total OA in the free troposphere during ATom-1 and ATom-2 as computed by the GCM12-, CESM2-, and CESM1-CARMA models.

https://doi.org/10.5194/acp-2019-773
Preprint. Discussion started: 20 September 2019

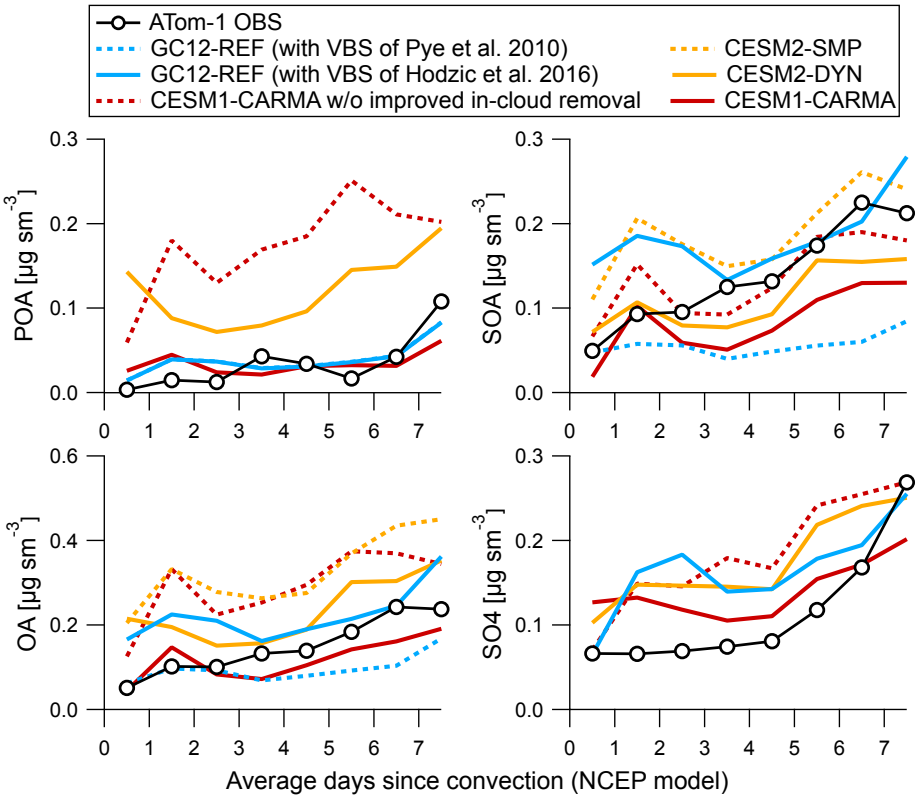

Figure 8: Measured and predicted mass concentrations of POA, SOA, OA and sulfate aerosols during ATom-1 as a function of the number of days since the air mass was processed through convection (based on a trajectory model from Bowman, 1993, and satellite cloud data from NASA Langley, https://clouds.larc.nasa.gov/). CESM2-SMP and CESM2-DYN have the same emissions and processing of POA and sulfate, and thus similar concentrations. The same is true for the two versions of GC12.

https://doi.org/10.5194/acp-2019-773
Preprint. Discussion started: 20 September 2019

(a)

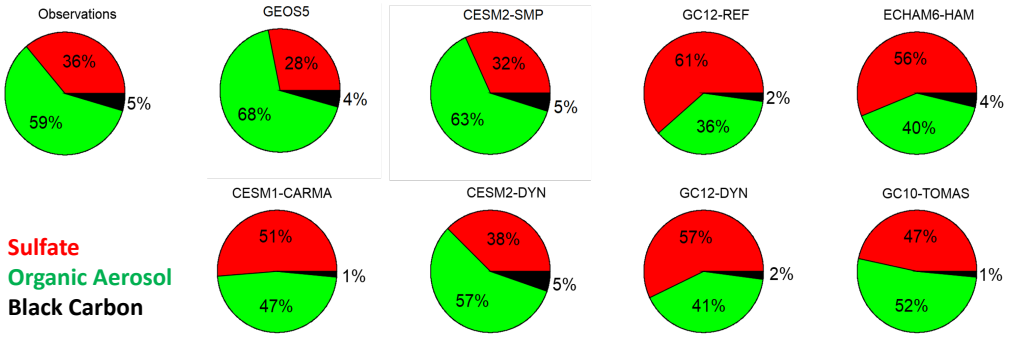

(b)

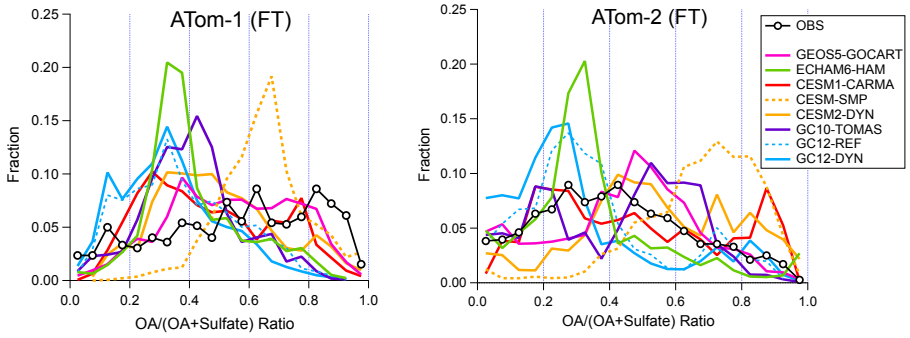

Figure 9: (a) Predicted and measured composition of submicron aerosols in the free troposphere as a function of the submicron aerosol mass concentrations during ATom-1. (b) Frequency distribution of observed and simulated ratio of organic to organic plus sulfate aerosols in the free troposphere during ATom-1 and -2.

https://doi.org/10.5194/acp-2019-773
Preprint. Discussion started: 20 September 2019

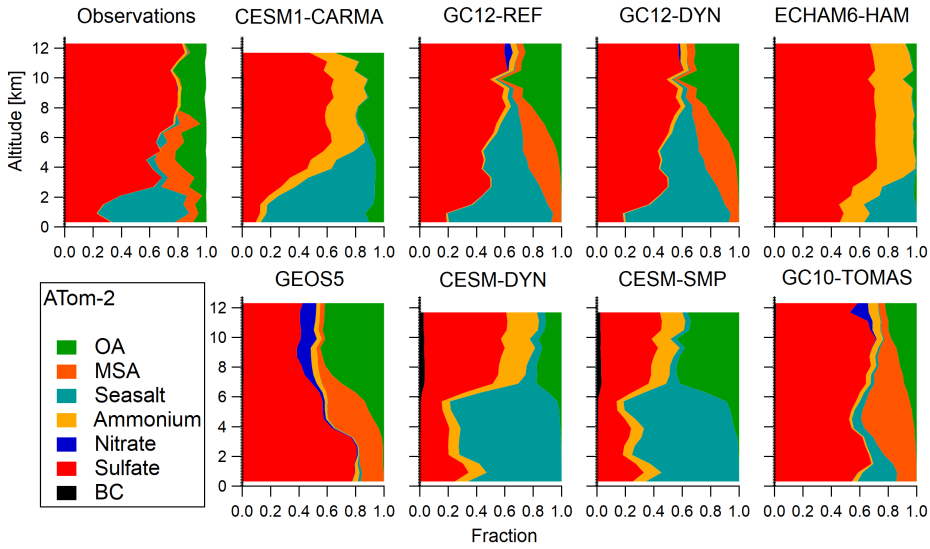

Figure 10: Comparison of measured and predicted composition of submicron aerosols as a function of altitude over the remote Southern Ocean region during NH Winter (ATom-2). For models that do not calculate ammonium in the aerosol (such as CESM1-CARMA, CESM2-SMP, CESM2-DYN and ECHAM6-HAM), ammonium was estimated from the sulfate mass assuming the formation of ammonium sulfate. Note that based on the PALMS measurements there is a small contribution of dust (~2% in the LS, negligible elsewhere) to the AMS size range, but since the accumulation mode dust in the models presented contains much larger sizes, it is omitted here to provide a fair comparison.